Unmanned Aerial System for Radioactive Source Search

A Thesis Presented for the

Master of Science

Degree

The University of Tennessee, Knoxville

William Lynch

May 2021

I would like to dedicate this paper to my friends, family, and faculty members who have been patient with me and provided countless amounts of help and support on this journey.

Acknowledgments

I would like to thank my teachers, staff, coworkers, and classmates that have helped me get to the end of this part of my educational journey. Specifically I would like to thank my committee members: Dr. Howard Hall, Dr. Lawrence Heilbronn, and Dr. Jason Hayward for their patience and understanding. They have been instrumental in my growth as a nuclear engineer through their classroom instruction and mentorship. I would like to thank my coworkers Dr. Benjamin Magocs and Isaac Stone for the work they have contributed to the SWARM project, for the countless late nights and working through a once in a century pandemic to see it through. I would also like to thank Dr. Matthew Cook for his tireless efforts in making sure my coworkers and I had the material and the support we needed to conduct this research. I also thank him for his mentorship and advice in writing this thesis. Most of all, I would like to also thank my parents and family for supporting me continuously in my education and life. Without the the support and funding from the Defense Threat Reduction Agency(DTRA), this research and thesis would not have been possible.

Abstract

A novel system of airborne radiation survey and source localization was built and tested. In the United States the National Nuclear Security Administration is currently using a two-tier approach that uses a manned fixed wing airplane and manned helicopter to survey nuclear disaster zones. The novel system proposed takes the operators out of harm's way and allows for higher resolution radiation surveys at a lower cost. This proposed system also allows the operators to locate a source rapidly if a source is stolen or lost. The proposed system is configurable for most radiation detectors that are compatible with Python and a Raspberry Pi.

The system was designed to be vehicle agnostic, to utilize a configurable radiation survey and source localization sensor package that can take data from one or multiple vehicles with reduced ri0sk to personnel and more costly equipment. This system uses a Bayesian Area Exclusion method developed around a predicted source and background strength to reduce the search time and area.

When tested against differing source locations or strengths, and flight altitudes, this system has shown improvements in source localization for low level source isotopes using single and multiple vehicles. The Bayesian Area Exclusion method has also been tested and shown to reduce the time necessary to search an area with acceptable accuracy.

Table of Contents

List of Tables

List of Figures

Chapter 1

Introduction

Since the beginning of the Nuclear Era, there have been concerns over what to do if some radioactive material is released into the environment or what happens if its stolen or lost. Both concerns are intrinsically linked, as methods used to map a distributed source or to localize a singular source are practically identical. Both problems require the deployment of one or multiple radiation detectors either man portable or carried by a vehicle to search an area and report the count rates identified by the detectors. Typically, source localization only goes one step further than a survey by identifying the maximum in the search area as the source. Historically there has been precedent for the concern about both problems.

As nuclear technology became more widespread, there have been concerns over what is to be done if some radioactive material is released into the environment and what happens if its stolen or lost. These concerns became ever more widespread as the Atomic Energy Act of 1954, allowed nuclear power and technology into the private sector. At the same time, the Cold War between the Soviet Union and the United States began and there are currently adversarial nuclear powers who may be willing to use nuclear weapons that scatter fallout over entire cities. During the Cold War, there were also numerous accidents at nuclear power plants and facilities that released radioactive material into the environment such as Three Mile Island and Chernobyl. Three Mile Island released primarily radioactive gases and Iodine-131 and there was an evacuation zone with a radius of 32.2 miles. The Chernobyl accident released radioactive gases, Cesium, Iodine, Strontium, and as much as 6 tonnes of the nuclear fuel in the core. This contamination produced an exclusion covering 2,600 km^2.

After the fall of the Soviet Union, the US became concerned with international terrorism. There have been rightful concerns about terrorist groups acquiring or producing a nuclear weapon and smuggling it into the United States for an attack. Even more recent than the War on Terror, there is the Fukushima Daiichi nuclear disaster which released radio-cesium into the atmosphere and groundwater. The evacuation zone in Fukushima covered a 20 km radius.

In response and anticipation of such events, the US government and many research teams have developed responses to the threat of a radiological release and lost or stolen sources as well as nuclear terrorism. The US's response is the National Nuclear Security Administration (NNSA)'s Aerial Measurement System (AMS) and Radiological Assistance Program (RAP). RAP is a ground-based resource while AMS focuses on the use of aircraft. RAP was developed in the 1950's as the NNSA's first responding resource to a nuclear emergency. They provide assessment, area monitoring, air sampling, exposure, and contamination control service in the event of a radiological release. RAP primarily uses field portable radiation monitoring instrumentation, mobile laboratories, and air sampling equipment. AMS was developed in the 1960's. This system makes use of two types of aircraft- fixed wing aircraft and helicopters. AMS are currently based out of Nellis Air Force Base in Las Vegas, Nevada, and Joint Base Andrews near Washington D.C. These aircraft carry radiation detectors while flying serpentine patterns over disasters zones. This system was deployed and used by the United States Forces Japan during the Fukushima Daiichi nuclear disaster to advise evacuation plans and track the movement and extent of the contamination. The large areas of evacuation and exclusion zones necessitates some method of rapidly and accurately surveying an area.

Since the NNSA's responses to a radiological release or the threat of nuclear terror all involve sending personnel into harm's way, a way to mitigate risk would be to begin to use unmanned vehicles. This new response would need to be configurable to the task at hand such as being able to be configured to discriminate between gamma and neutron emissions or identify the radioisotopes present. Due to the wide array of detectors available, there is a need for a standardized detector package system that contains all the electronics to record the detector and GPS data, to pilot the vehicle, and to transmit the findings to a ground station. The package should also include the power system for the detectors, communications, and computer system and must be capable of fitting on various ground and air vehicles. The proposed system should also be made using off the shelf components to reduce cost. This system will need to develop and utilize data analysis tools and methods to interpolate between data collection points and to identify the exact positioning of the source. The project will use multiple tiers and search methods to correctly identify a radioactive source in a known area similar to AMS. Preferably these search methods will differ to eliminate any potential error stemming from the use of one method.

Chapter 2

Literature Review

In the years after the Fukushima Daichii disaster, many research teams have been putting together airborne radiation detection systems to expand radiation dose mapping and source tracking capabilities to assist with the remediation and cleanup of the region. In addition to cleanup work, some projects have been developing source localization techniques using an aerial vehicle to assist in finding larger concentrations of radioisotopes and these systems also have a potential use in nuclear security.

2.1 Radiation Survey and Dose Mapping

Since the advent of the Nuclear Era, there has been the possibility of a catastrophic event that ends up scattering radioactive material over a large area prompting the question of how one would track and measure it. In the 1960's the National Nuclear Security Administration response to this question was the Aerial Measuring System(AMS) tasked "to provide real time measurements of low levels of air and ground contamination" and "to provide a rapid survey of radiation and contamination following a radiological emergency" [6]. Their goal for using an airborne system was to provide a more efficient, cheaper, and safer survey method than more traditional static or ground mobile systems. While more effective than a ground based system, there is still risk to the pilot and crew, which prompted research teams in the early 2000's to begin investigating mounting radiation detection systems to unmanned aircraft. In addition to improving operator safety, a move to an unmanned system would make the system cheaper and potentially easier to deploy.

2.1.1 Platform

The platform choice has a great effect on the speed and resolution of the surveys produced by the system. For this project there will be two classifications of aircraft: fixed wing and rotary wing aircraft. On average fixed wing aircraft must maintain a high speed and altitude which can increase the area covered but can result in lower resolution surveys. In comparison rotary wing aircraft such as helicopters or multi-rotor vehicles move slower, can hover, and are able to safely reach lower altitudes which can produce slower but higher resolution surveys. A 2017 AMS report states they uses a fixed wing Beech King Air B-200 and a Bell-412 helicopter. The AMS Beech King could survey a 64.75 km^2 area with between 1.6 to 8.04 km spacing and with an altitude of between 152 to 609 m. This vehicle has a mission speed of 72 m/s and a flight endurance of 2100 km. The AMS Bell-412 can cover the same area with 30 to 48 m spacing at altitudes between 15 and 152 m. The mission speed for this vehicle is 36 m/s. Both vehicles are manned and powered by combustion engines. The area covered and survey times of the AMS system can be viewed as a control for any future unmanned aerial detection system to beat.

Fixed Wing

The primary reasons for choosing a fixed-wing aircraft are the speed, endurance, and payload capacity which generally outperform the rotary-wing aircraft. Despite these benefits there are downsides to a fixed-wing aircraft such as wider flight path spacing, higher required minimum altitude, as well as the infrastructure required to take off and land. Appendix B Table B.1 gives a break down of the characteristics of fixed wing survey vehicles

The research team behind "The Design of A Radiation Surveillance Unit for an Unmanned Aerial Vehicle(UAV)" decided to use a fixed wing Ranger UAV for their platform [13]. The Ranger has a flight endurance of 6 hours and a range of 180 km. It has a maximum payload weight of 45 kg and a wingspan of 5.71 m. This drone comes with an automatic launcher that can be mounted to a truck for less strict requirements for takeoff and landing space.

In “Airborne Radiation Mapping: Overview and Application of Current and Future Aerial Systems” the researchers state that the lowest cruising speed of an unmanned fixed wing aircraft is 17 m/s which assuming a data collection rate of 1 Hz translates to a 17 m per measurement spatial resolution [9]. This article noted there are manned Vertical Takeoff and Landing(VTOL) vehicles that can takeoff, land, and hover like a rotary wing aircraft, and can cruise like a fixed wing aircraft. However, they were unable to do any testing on a VTOL vehicle. The research team’s system uses two tiers one of which would use a fixed-wing unmanned aircraft like AMS for a quick low-resolution survey of a larger area. The other tier is a helicopter which is used for a finer detailed survey.

Rotary Wing

The primary reasons for choosing a rotary-wing aircraft are the ability to hover, tighter flight paths, lower minimum altitude, higher stability, and the ability to take off and land vertically. The downsides of the rotary-wing aircraft are lower speeds and reduced area covered. To take off and land, this category of aircraft only needs enough space for the props to avoid colliding with anything, which is significantly smaller than an airfield. The characteristics of the rotary wing vehicles from the following articles and journals are compared in Appendix B Table B.2 and B.3.

As previously stated, “Airborne Radiation Mapping: Overview and Application of Current and Future Aerial Systems” used a smaller rotary wing unmanned aircraft for its second tier to make a finer resolution survey over the hot spots detected by the fixed wing aircraft [9]. The researchers chose the helicopter to cover hot spots for its inherent ability to hover and move slower than the fixed wing aircraft. The rotary wing vehicles covered in this article were able to fly at velocities as low as 1.5 to 8 m/s and featured increased stability when compared to fixed wing vehicles. This class of vehicle does not need a professional pilot and is easy to use even in adverse weather conditions. The article indicates that the greatest impacting factors on the quality of the survey are the mission altitude and the velocity of the vehicle.

A lithium polymer battery powered multi rotor UAV is used in the system described by "3D Unmanned Aerial Vehicle Radiation Mapping for Assessing Contaminant Distribution and Mobility" [2]. It was developed by the University of Bristol (UK) and has a flight endurance of 30-35 minutes. Due to the airspace regulations in the UK, the total mass of the vehicle was limited to 7 kg and in order to maintain the flight time the package capacity was limited to 500 g. This vehicle was capable of achieving altitudes between 1-20 m. The flight spacing was between 2 and 2.5 m.

In "Aerial Radiation Monitoring Around the Fukushima Daiichi Nuclear Power Plant Using an Unmanned Helicopter", the team focused on helicopters initially wanting to use a manned one but were constrained by Japanese regulations requiring a manned helicopter to fly no lower than 150 m above ground level [8]. Given that Japan makes frequent use of unmanned agricultural helicopters, the project adapted to use a Yamaha Rmax G1. This model is a gasoline powered vehicle with a maximum practical payload of 10 kg. The vehicle itself weighs 94 kg and has a maximum speed of 20 m/s and a total flight time of 1.5 hours.

The article, "First Demonstration of Aerial Gamma-Ray Imaging Using Drone for Prompt Radiation Survey in Fukushima", discusses two different classes of vehicle: the unmanned helicopter and the unmanned multi rotor [17]. Initially they had planned to use the unmanned helicopter, but the cost caused the team to switch to a multi rotor UAV, the DJI S1000+. The price of the helicopter was $1,000,000 while the DJI cost only $6000. There was a significant size difference between the two vehicles with the helicopter being 3.63 m wide and the DJI being 1 m wide. This size difference also affects each vehicle's maximum payload and flight endurance. The helicopter could carry 10 kg for 90 minutes while the DJI only could carry 5 kg for 10 minutes.

There were two drones used over the course of the testing conducted in "Use of Multi-Rotor Unmanned Aerial Vehicles for Radioactive Source Search" [37]. These two drones were the DJI Matrice 600 and 100 with the 600 being the original choice and the 100 being used for the smaller testing area. The DJI Matrice 600 is a hexacopter with a maximum speed of 18 m/s and can maintain a mission altitude of 10 m. The 600 has a maximum payload of 5.5 kg which allows for a maximum flight time of 18 minutes. This flight time increases to 30 minutes with the payload of sensors used for this test. The Matrice 100 was only able to maintain flight for 16 minutes and has a much lower maximum payload of 1.25 kg. The testing site was reduced to a smaller area, and therefore, the Matrice 600 was replaced with the smaller Matrice 100. This vehicle has a flight time of 15 minutes with the detector payload.

2.1.2 Sensor Package

The sensor package can be defined as all the electronics, computers, sensors, and radiation detectors that allow a system to collect the necessary data. This package can either store the data locally on some storage device or transmit the data to the ground station in order to provide real-time results. These systems can also be responsible for controlling the host vehicle or the vehicle can be operated by a remote pilot. The system must include a GPS unit and radiation detectors and can have additional sensors like Lidar or 3D cameras to provide contextual information to the crew about the area. The quality and quantity of the sensors are restricted by the vehicle one chooses to use. Detectors made from certain materials can be negatively impacted or break under constant vibration, thus the type of scintillator crystal chosen may be influenced by the vehicle used. In the control case of the manned AMS system, the fixed wing vehicle and helicopter carry different payloads. The fixed wing vehicle carries two of the packages, while the helicopter carries four. The packages are produced by Radiation Solutions, Inc and contain two-liter NaI crystals, four RSI 701 acquisition systems, two RSI-501 aggregator systems, and two DOE Spectral Advanced Radiological Computer Systems. The aircraft can also carry a mechanically cooled ORTEC HPGe Detective-Exs for high resolution spectroscopy and two Canberra ADM-300 health physics kits to monitor the safety of the crew.

"Airborne Radiation Mapping: Overview and Application of Current and Future Aerial Systems" discusses many of the different types of scintillator crystals and the addition of secondary contextual sensors [9]. The most common types of scintillators are lanthanum bromide doped with cerium (LaBr3[Ce]), sodium iodide (NaI), and cesium iodide (CsI). NaI and CsI detectors are said to be quite similar. NaI is cheaper and more commonly found than CsI, but it degrades upon contact with water. CsI is also noted as being less brittle which prevents damage from the mechanical vibration of the vehicle and potential shock. CsI is recommended and selected due to these mechanical properties as well as having a higher gamma absorption coefficient which allows a smaller crystal to be used. $LaBr_3[Ce]$ is not recommended as there are degradation issues with water similar to NaI. $LaBr_3[Ce]$ has poorer peak shaping which makes it is more difficult to identify isotopes. Poor shaping performance is considered less of a problem in post-disaster zones as the common radionuclides are well known. CZT's is also listed a possible alternative due its very high mass number and good counting efficiency. The manufacturing process for this crystal is somewhat flawed and imperfections in the crystal are commonly produced in larger crystals. There is future work covering ultra-dense semi-conductor materials like diamond or uranium dioxide. Besides these semi conductors, gamma imaging is alternative method which produces two dimensional images from the gamma rays on a NaI target. The concerns for this system include the need for a higher activity over the period of exposure and the weight of its lead collimators. Both Lidar and stereovision cameras have been tested in the 3D mapping applications of this system. A single point range finding Lidar system was found to increase the accuracy of the on-board altimeter and GPS. The stereovision cameras were combined with prior maps of the area to find the altitude of the vehicle. This journal suggests that there is still more work needed to provide accurate three-dimensional models of radiation distribution. This work will primarily involve integrating 3D scanning Lidar and stereo vision. In total this system will provide a cheaper, better resolution, and safer alternative to the AMS manned system as well as a much faster alternative to traditional ground-based monitoring and surveys.

The package from the article,"Design of a Radiation Surveillance Unit for an Unmanned Aerial Vehicle", consists of a Geiger–Müller (GM) detector, NaI detector, a CZT detector, an air sampling unit, environmental sensors, on board computer, and GPS receiver [13]. This package is designed to track plumes from the back of a high endurance fixed wing drone and each of the sensors serves a specific purpose and provides crucial details about the plume. To find the dose rate, a traditional Geiger–Müller tube is mounted. The selected model features two tubes with a high and low dose rate meters. The range of this detector is 0.01 Sv/h – 10 Sv/h. A NaI scintillator was chosen to localize the plume. The crystal of this scintillator is restricted to 150 mm x 100 mm due the requirement that the system replaces the traditional sensor suite of the drone. HPGe detectors were initially considered but due to the need for mechanical cooling and its large size, it was struck from the final design. This system was also concerned with the scintillator being overwhelmed and useless from inside the plume, so a CZT compound semiconductor was chosen to identify isotopes inside the plume. This crystal was 5 mm x 5 mm x 5 mm which limited its high energy gamma efficiency. This crystal was mounted inside the air sampling unit to account for its low efficiency. The air sampling unit was equipped with a fiber and charcoal filter and with its inlet facing toward the front of the Ranger. This package was powered from the vehicle and had its own internal computer and communication systems.

In "3D Unmanned Aerial Vehicle Radiation Mapping for Assessing Contamination Distribution and Mobility", the detector package consisted of a Kromek 1 cubic cm spectrometer [2]. This spectrometer has an energy range of 30 keV to 3 MeV. This detector also had an energy resolution of 2.5% at 622 keV. The Lidar unit for this system was a 3D gyro stabilized single point laser rangefinder with an accuracy of 5 cm within its 0.2 m to 30 m range. The Lidar,GPS, and spectrometer were sampled every 500 ms and this data was recorded onto an Arduino ADK.

The radiation detection system designed in "Aerial Radiation Monitoring Around the Fukushima Dai-ichi Nuclear Power Plant Using an Unmanned Helicopter", weighs 6.5 kg and uses three $LaBr_3[Ce]$ scintillator detectors with 38.1 mm diameter and 38.1 mm length [8]. This system is electronically insulated from the vehicle and no noise was detected during testing. During the experiment, the researchers recorded the count rate of the three detectors, and the spectral and positioning data. The spectral data range on the MCA was between 0 to 3000 keV, but all counts were included in the count data. The pulse height discriminator eliminated any counts less than 50 keV. As the energy of the gamma emitted from Cs-137 is 662 keV, the full width half maximum over the peak of 662 keV was noted as 2.8 percent. This was deemed acceptable enough to discriminate between Cs 134 and 137. This data was sent over a WLAN connection to a laptop to provide a real time map.

The "First Demonstration of Aerial Gamma-Ray Imaging Using Drone for Prompt Radiation Survey in Fukushima" system is unique for featuring a Compton camera instead of a traditional scintillator [17]. This package also contains the various electronics to record and transmit the data to a ground station. The Compton camera is noted for having a wide field of view and not needing a mechanical collimator or coded mask. The model of Compton camera used was developed at Hamamatsu Photonics and weighs only 1.9 kg and is 13.5 cm x 14 cm x 15 cm and features a fish-eye lens. The scintillator crystal for this camera was a Ce:GAGG material which features a high density, high light yield, and no internal background interference. This model is so sensitive that it can image 1 MBq of Cs-137 from 50 cm in 10 seconds which is 0.35 Sv/h. The maximum payload for the drone is 11 kg but considering the batteries which weigh 2 kg, the detector suite maximum weight is 4.6 kg. A GPS, accelerometer, and speedometer are also installed. With these systems installed the horizontal and vertical position accuracy is 1.5 m and 0.5 m. The wireless system allows communications up to 1.2 km away. A Raspberry Pi Intel edition records the data from the camera and Compton camera and transmits the information to the ground station. Due to concerns about an unstable power supply, the Pi was replaced with a laptop.

2.1.3 Testing Methodology

The testing methodology criteria for all of these systems are how much area the system can cover, and how fast and accurate are the resultant surveys. These criteria can be affected by the vehicle's design, flight endurance, speed, and flight path as well as the quality of the detectors, electronic polling rates, and the additional electronics in the package. Since the AMS was deployed and used during the initial response to the Fukushima Daiichi disaster and has been tested against ground-based systems, its performance will be used as a standard to compare with the unmanned systems' results. AMS competed against the Ground Mobile System by having both systems surveying a 1-mile by 1-mile area. AMS's fixed wing aircraft was flying 152.4 m above the ground with spacing of 304.8 feet at a speed of 240 m/s. The comparable GMS completed the same mission at 0.9 m above the ground with spacing of 18.3 m at 60 mph. The fixed aircraft took 5 minutes while the GMS took 132 minutes. AMS's helicopter completed its higher detailed survey at 67.1 m above the ground, with 134 m spacing and a mission speed of 35.8 m/s. To achieve a similar level of detail the GMS test was conducted at 0.9 m above the ground with 18.3 m spacing but at a lower speed of

13 m/s. The results from the final survey were that the helicopter took 22 minutes and the GMS took 220 minutes.

When deployed to Fukushima, the packages were mounted on United States Forces Japan (USFJ) military aircraft which required some modifications to host the packages. Normally the packages are powered by the aircraft, but the military vehicles were unable to power the system thus batteries had to be improvised. The packages were also further modified to contain an extra module to measure airborne contamination. The deployment of this system was also hindered by the USFJ pilots being unfamiliar with the specific flight patterns required for this system. From March 17th to the 19th, AMS mapped the area within the 30km radius evacuation zone and resultant data was published on the 22nd.

There were two tests performed in "First Demonstration of Aerial Gamma-Ray Imaging Using Drone for Prompt Radiation Survey in Fukushima" [17]. These tests compared ground methods of surveying to the aerial surveillance system the team had designed. The proposed aerial system and ground surveys are tested in the same schoolyard in Fukushima. This yard is 80 m x 100 m and has partial tree cover. The intended goal was to create an air dose rate map of the school yard. The ground-based portion of this survey consisted of making a 6 x 5 grid in the schoolyard with 20 m spacing. At each point in the grid, the air dose rate was measured 10 times within a 2 m circle of the point at a point 30 cm above the ground. The time for each point was 5 minutes and it required 30 minutes of total walking time. In total this measurement took three hours. The detector used was a scintillator-based survey meter, Furukawa Co Gamma Spotter. A spline interpolation was used to generate a field map but can be considered inaccurate due to missing some hot spots between the grids. It was noted that there were missed hotpots between the grid of measurement points. This error could have been reduced by making the grid closer but would have increased time requirements.

This testing used a Compton camera to image the same school yard as before. Flights were taken at 10 m and 20 m altitudes. The 10 m flights took 11 and 14 minutes and were able to get 50 m diameter snapshots. The two 20 m flights took a combined time of 25 minutes and 9 seconds. This flight was able to get a snapshot of a 100 m diameter circle with reduced spatial resolution due to increased distance and wind moving the drone. The achieved spatial resolution was 4 – 10 m. Using the aerial method took a significantly shorter amount of time to map the same area. It was found that the aerial maps are qualitatively consistent with the ground-based surveys. It is noted that an aerial system reduced the measuring time by a factor of 10. This aerial system also found hot spots around the search area. It is also noted that the altitude severely affects the accuracy of the maps generated. The journal also notes that there is future work to be done in a revised altitude control system and improving the conversion from the Compton camera output to the map.

The system from "3D Unmanned Aerial Vehicle Radiation Mapping for Assessing Contamination Distribution and Mobility" was tested at a stepped farm within the 35 km exclusion zone of Fukushima [2]. This farmstead was within the north-eastern area of Fukushima province that was heavily impacted by the contamination. This test site has dimensions of 200 m x 50 m. The UAV's Lidar and GPS are used to generate a topographical map of the area and collected counts normalized to a height of 1 m above ground level. The data from the flights was run through a geospatial analysis software that generated an XML file with longitude, latitude, altitude, and counts per second. This system was able to produce a highly accurate map of the 1,000 m^2 area within a single 15-minute flight.

2.2 Source Localization

The advent of the Nuclear Era spawned the need for radiation surveying technology, there has been similar need for quick and accurate source localization technology. Source localization is very similar to survey mapping but has the end goal of locating a radioactive source for identification instead of just mapping the count or dose rates in an area. This is typically achieved by initially surveying the search area and interpolating between data collection points and identifying the highest count rate position in the search area. This need was exacerbated by the fears of nuclear war and terrorism in which one may need to quickly locate a nuclear weapon or device once a threat has been identified. This kind of system and technology is also needed in the area of nuclear security. Using this type of system, allows the operator to quickly identify, if a state actor is complying with international safeguards and nonproliferation regulations. There is also need for this technology in the fields of decommissioning and waste management as one may want to ensure there are no sources left behind or finding a lost or stolen source.

2.2.1 Platform

As with the other section dedicated to platforms, this section will discuss primarily the rotary wing aircraft chosen by research teams. Rotary wing aircraft are chosen primarily for their abilities to hover in place as well as to fly tighter spacing flight paths than fixed wing aircraft. In addition to the reasons previously stated, one might also chose an airborne system for source localization in the international safeguards and nonproliferation role to reduce the risk to agents who would otherwise have to be there in person and instead send a remotely operated vehicle.

The detector suite from "3-D Radiation Mapping in Real-Time with the Localization and Mapping Platform LAMP from Unmanned Aerial Systems and Man-Portable Configurations" is mounted to a DJI Matrice 600 UAV [1]. This vehicle has a flight time of 1 hour with a payload of 4.5 kg and with a payload of 6 kg the flight time reduces to 20 minutes. It can then be said that for smaller unmanned rotary wing aircraft payload can significantly influence flight time and thus the amount of area surveyed and resolution of the survey.

In "Use of Multi-Rotor Unmanned Aerial Vehicles for Radioactive Source Search", the research team also made use of an unmanned multi-rotor, a DJI Matrice 600 [37]. This vehicle has a size of 1668 mm x 1518 mm x 727 mm and a payload capacity of 5.5 kg. Its lithium polymer batteries have a capacity of 5,700 mAh which provide the drone with an effective flight time of 18 minutes with a full payload. This flight time would increase to 30 minutes with a payload used for the rest of the test. Due to the size of the available testing ground, the team swapped the Matrice 600 for a Matrice 100 which is about a half the size of the 600. The Matrice 100 has a flight time of 15 minutes with the detector payload.

2.2.2 Sensor Package

The requirements for a source localization sensor package are very similar to those used for a surveying or dose mapping package. The radiation detectors must be capable of detecting whatever source is being looked for as well as be robust enough to withstand the vibrations and rigors of flights. These detectors also need to be large enough and of high quality so that they can detect a potentially shielded source. As stated, before these packages can either be pure radiation detectors or can feature additional sensors to provide contextual information about where the source might be.

The payload described in "3-D Radiation Mapping in Real-Time with the Localization and Mapping Platform LAMP from Unmanned Aerial Systems and Man-Portable Configurations" as the Localization and Mapping Platform(LAMP) and is a platform agnostic, self-sufficient system with a variable sensor configuration [1]. Both descriptions mean the payload can be carried by a person, ground vehicle, or air vehicle without a need for an external power source. The payload consists of a laptop with Intel i7 processor, power distribution system, a Velodyne Puck Lite Lidar, Vectornav 300 inertial navigation system, visual camera, and 131.1 cubic centimeter CsI(Tl) scintillator volume. It was calculated that 27 percent of the weight of the payload was detector weight.

The sensor package in "Use of Multi-Rotor Unmanned Aerial Vehicles for Radioactive Source Search", is responsible for data collection as well as piloting the vehicle [37]. The main control module is responsible for piloting the vehicle by sending commands to the flight computer mounted on the drone. This module is also sent data from the radiation detector sensor at a sampling rate of 1 Hz. This system also uses a 433 MHz radio system to transmit collected data and communications with the ground station. There is also a camera which transmits over a 2.4 GHz wireless link to the remote controller. The ground station computer transmits search area parameters like the width, the length, the altitude, and the speed. This central processor unit is a BeagleBone Black development board with 4 GB of flash storage.

The radiation detection suite is an ARD100 from Shanxi Zhongfu Nuclear Instruments Co. This is a dual detector scheme with one low range detector capable of 0.1 Sv/h to 0.6 mSv/h and a high range detector capable of 0.6 mSv/h to 1 Sv/h. As implemented the total range of the system is 1 Sv/h to 500 mSv/h. The detection sensitivity of this system is 100 cps / Sv / h. The lower range detector uses a silicon photodetector and CsI(Tl) crystal. The crystal's dimensions are given as 15 mm x 15 mm x 15 mm.

2.2.3 Testing Methodology

The key testing criteria for any localization system is how fast and accurate the system can identify various strength sources in a variable sized area. Naturally, the source used for testing ought to be tested with it shielded and unshielded. The detection packages also should be sensitive to the type of radiation emitted by the source. If there are contextual sensors like cameras or Lidar units, data from those sensors ought to enhance the ability of the research team to retrieve the source once the system has identified it.

The LAMP system from “3-D Radiation Mapping in Real-Time with the Localization and Mapping Platform LAMP from Unmanned Aerial Systems and Man-Portable Configurations” was tested three times with one test having the source located inside of a building, one with the source in an open field, and a distributed source in a field [1]. For the test finding a source inside of a building, a 400 micro Ci Ba-133 point source was used with it up against a window. The LAMP system was flown around the building in 6 minutes covering the 5 x 5 m building. The resultant count rate data was projected onto a 3D image taken by the system. This test results showed a local hot spot with counts centered around the correct window with the source against it. The second test with source in an open field made use of the same 400 micro Ci Ba-133 source. The testing area was 30 x 20 m. The drone was flown in a serpentine path at an altitude of 2.5 m and resultant count rate data was plotted over a 3D image taken by the vehicle. For this test, the system took only 8 minutes to collect this data. The third test made use of a contaminated field in the Fukushima exclusion zone. This test did not make use of a drone but was handheld by a researcher about 1 m off the ground. The researcher also followed a serpentine path over a 6 x 56 m area. This test was able to localize two hot spots where Cs-137 in water that had collected in a water drainage area in 4.5 minutes.

There are three different search patterns tested in “Use of Multi-Rotor Unmanned Aerial Vehicles for Radioactive Source Search” : Traversal, Binary, and Successive [37]. The Traversal is the standard and most used search pattern. The pattern can also be called a S-pattern which crisscrosses over the search area. The on-board computer then calculates the maximum dose rate in the area and hovers over the location to alert the operators.

The Traversal pattern has a time complexity of O (n^2). The Binary search pattern begins with three flights over both longest edges and then their bisector. The mean dose rate is then calculated and compared. The lowest mean is discarded and then the remaining two become the new borders of the search area. The shortest edges and their bisector are then measured and the same process of discarding and shrinking is continued till the GPS becomes inaccurate. This method decreases the time complexity by removing half of the search area each time and can achieve O (log N). The Binary method did require a higher activity than the Traversal method. The Successive Approximation method uses the assumption that a source produces a circular field and the theory of the perpendicular bisector. The vehicle flies over the longest edge of the search area first and calculates the position of the maximum dose rate. Once the drone flies to this location and perpendicularly cuts into the search area and finds the local maximum. The Successive method also requires a higher activity than both Traversal and Binary search patterns but can reduce the time complexity to O (1).

The testing was performed with the Shanghai Station of Radiation Environment Supervision at a municipal radioactive waste repository. This testing site measured 30 m x 25 m and had no trees. The vehicle was downgraded to a DJI Matrice 100 instead of the 600 due to the smaller size of the testing site. The sources used were four Am-241 sources with an activity of $3.7x109$ Bq. This activity was considered unusable to test the Binary and Successive search methods. Since the radiation detector polling rate was 1 Hz, it was found that the lower the vehicle speed that better the search accuracy. The flight time of the Matrice 100 UAV with the detector suite was limited to 15 minutes, thus the test used an altitude of 10 m, a spacing of 1 m, and cruising speed of 1 m/s. The first test was conducted without sources to check for drift and stability in the platform. The source was placed randomly in the search area and then the second flight was started. This data was exported and plotted in MATLAB. This took three minutes to interpolate between data points and plot the map. The system was accurately able to identify the highest dose rate location in the search area which corresponded with the location of the source. The location of the highest dose rate was (15.1, 14.3) which when compared to the location of the source (15, 14) resulted in a location error of 0.32 m. This could be due to the source being shielded in an open top lead cylinder container which permitted a strong dose rate only above the source.

The batteries used were also capable of providing power over the 15-minute flight. This article concludes with a review of the drone and its advantages in take-off and landing site requirements, and ability to hover. It also discusses possible future work which will include an improved resolution and efficiency as well as a manipulator which can grab sources. They also have plans to test with multiple sources in a testing area and with multiple drones.

Chapter 3

Materials, Methods, and Approach

3.1 Sensor Package

The sensor case contains all the necessary electronics to collect gamma or neutron radiation data, record, and transmit this data to the ground station as well as calculate flight paths for the vehicle.

3.1.1 Case

The case is the container for all the components. It is a J-314 blow molded plastic case made of high-density polyethylene with custom designed polyurethane foam cushioning. The case has outer dimensions of 711 mm x 229 mm x 114 mm and internal dimensions of 679 mm x 197 mm x 67 mm with a lid depth of 29 mm. Two 2 mm holes have been drilled into the case in the slot for the radios to allow the antennae to have line of sight to the corresponding pair on the ground station laptop.

3.1.2 Raspberry Pi

The microcomputer chosen for this project is a Raspberry Pi 3B+. This microcomputer has 4 USB 2.0 ports and 1 Ethernet port. Its CPU runs at 1.4 GHz and has 1 GB of RAM. This Raspberry Pi is powered by the primary USB power bank. The OS loaded onto the Pi is Ubuntu 18. This computer system is responsible for handling communications between the ground-station and the vehicle, plotting the course, and collecting and transmitting the detector data, GPS positioning, vehicle battery life, and CPU temperature. The microcomputer communicates to the drone mounted Pixhawk flight computer over a micro USB cable. The Raspberry Pi is powered by a 2.1 mA, 5 V, 10,000 mAh power bank battery.

3.1.3 Detector

The current implementation of the detector scheme is: 1 2.54 cm height x 2.54 cm radius right cylindrical EJ-276 scintillator crystal with Bridgeport Instruments (BPI) USB Base; and 1 Osprey NaI scintillator detector. The Bridgeport plastic detector transmits data and is powered by the USB on Raspberry Pi while the Osprey NaI detector is powered by the secondary USB power bank and transmits data via the Ethernet port on the Pi. The BPI detector with its plastic scintillator has an intrinsic efficiency for 662 keV gammas of 35% and is the primary detector used for this system. The dimensions of the volume dedicated to detectors is 14.7 x 36 x 5.7 cm and the foam can be redesigned to accommodate any detector capable of fitting in that volume.

3.1.4 Xbee Radios

This vehicle mounted package communicates with the ground station laptop over a serial connection using two pairs of Digi Xbee Pro S3B 900 MHz radios. These radios and antennae must have a direct line of sight for optimal signal strength. As a result of this two 5/64“ holes were drilled into the bottom of the cases to allow the antennae a line of sight to the ground station radios. With a good line of sight, these radios have a range of 402 m with a 100% transmission rate. The testing performed on this system was limited by the testing area and is possibly not the final range of these radios. In Appendix C Figure C.1 highlights the components of the package.

3.2 Drone

While this system is designed to make use of any Pixhawk compatible vehicle with sufficient payload capacity, a HL-20 was used for the purpose of design and testing. The HL-20 has a wheelbase diameter of 144.78 cm, a height of 66.04 cm, and an empty weight of 9.525 kg. This vehicle is a hexacopter and can carry a max payload of 19.96 kg, but this would exceed FAA regulations of "Exception for Recreational Flyers" which limit drone takeoff weight to be less than 24.95 kg. If the payload of the HL-20 is increased past the 24.95 kilograms, the pilot must have a Part 107 license. An additional constraint in designing the package was the drone's gondola opening of 255 mm x 195 mm. This drone has a max speed of 10.28 m/s and a max flight endurance of 60 minutes. The vehicle can operate between 0 and 1188 m above ground level and anywhere within a 1524 m line of sight distance. The folding arms and props to allow for easier and more compact transportation. This drone also comes with multiple safety features like redundant Pixhawk flight computers, GPS units, and a low battery mode which will return the drone to the launching zone or land the vehicle if it detects low battery. The redundant GPS units are configured in a differential GPS mode which allows for +/- 0.5 m vertical, and +/- 1.5 m position accuracy. The power source for this vehicle can be two or four 16000 mAh, 6S 22.2V DC Lithium Polymer (LiPo) batteries that can be swapped between flights for longer periods of flight.

3.3 Code for Communications, Data Collection, and Flight Path Generation

The sensor package is coded using Python 3.8. The code primarily uses packages from Dronekit, Digi Xbee, BPI Python libraries, and geodesic distance calculations. As Python is incapable of utilizing multiple CPU cores or having multiple processes running concurrently, there is heavy utilization of threading which queues tasks and allows for sharing of data across sections of the code. Due to this implementation and how the Dronekit library is written, the Dronekit vehicle object must be passed between these threads and locked and unlocked during use and this can put a limit on how often the drone is accessed.

3.3.1 Communications

The communication between the ground station laptop and the packages are handled by the Raspberry Pi and the ground station laptop and make use of the Xbee radios. Originally this system was designed around having constant contact between the ground station and a lead vehicle. This constant communication was designed to provide orders to that vehicle at a constant rate. These orders were derived from the vertical grid function that generated a list of flight way points over the search area. The follower aircraft kept constant contact with the lead vehicle and followed along as the lead vehicle moved. This proved a two fold problem: the vehicles were not autonomous, as well as if there were dropped packets between the laptop and packages, the vehicle could escape the control of the Python script and crash. Dropped packets are an issue as communication on this system is handled via UDP instead of TCP so there is no message received check. The simple solution to these problems is to move way point calculations to the Raspberry Pis after passing them the initial inputs to the vertical grid function. This critical information exchange happens only three times in the new system versus for every movement way point for the old. This has the effect of making the vehicles autonomous which adds resilience to dropped communication packets and should prevent crashing caused by no command escape errors. There are also issues with follower aircraft when moving to autonomous flight. In order to not have a collision, the vehicles would still need constant communication or be perfectly in sync with one another. This is mitigated by parallelizing the search pattern and dividing the search area equally among all available drones.

Changing from follower aircraft to a parallelized search pattern has also been achieved. This has the added benefit of reducing search time as the vehicles are not covering the same area multiple times. The vehicles are also operating on the same altitude and thus can have their count rates directly compared as opposed to a staggered follower system where the higher vehicle will receive significantly lower counts than the loWest altitude vehicle. Since the vehicles are autonomous the separated search areas also provide a safeguard against accidental crashes if there is a delay in communications which could cause the vehicles to collide.

As previously mentioned the vehicles are now autonomous and this is achieved by passing the initial data to the vehicle from the ground station and having the vehicle calculate its own way points. This process is repeated for all vehicles as each vehicle now has two radios paired with two on the ground station laptop. Each side of the communication has a radio dedicated to transmitting and receiving. This is done to prevent messages from being lost if a single radio is receiving and attempting to broadcast simultaneously. The laptop is the limiting factor on the number of drones. The laptop must have two USB ports for the two radios per vehicle. Thus the communication diagram for the system as implemented looks is represented below in Appendix C Figure C.2.

This revised communications system has been redesigned to use command and status flags. The command flags are sent from the ground station at take off and the beginning or end of a tier. The status flags are how the package lets the ground station know what it is doing and what is the current tier. The status messages are sent every 0.2 seconds in a tier and every second when flying between tiers. The Appendix C Table C.4 presents the status and command flags as well as their definition and context.

Originally the communications were encoded but did not have any form of error correction. In effort to combat dropped status messages the communications between the ground station and packages are encrypted via SHA-256-bit Hash. This serves double duty by providing security and error correction as each message sends the Hash value and the decoded message with commands to throw out any received message in which the Hash and message do not match. In each status transmission, the vehicle sends the Hash value, vehicle index, GPS latitude and longitude, altitude, BPI count rate, vehicle battery level, and Raspberry Pi CPU temperature. Commands are sent to a specific vehicle based on a list of vehicle indexes derived from the vehicle names. The takeoff command sends a Hash value, vehicle index, and command flag of ”T“. For tier commands, the ground station laptop will send a Hash value, command flag for the tier, and the initial data such as the South West most point’s latitude and longitude, search width and height, spacing, and altitude.

3.3.2 Data Collection

The data collected by this sensor package is the GPS latitude, longitude, and altitude, BPI count rate, vehicle battery level, and the Raspberry Pi CPU temperature. The most important data reported are the GPS position, altitude, and the BPI count rate. Much of this data is reported by the vehicle over the USB cable between the Raspberry Pi and the Pixhawk flight computer. The vehicle data is reported by Dronekit commands and passed between the flight path thread and the data collection thread. Thus, the GPS position and altitude are recorded every 0.2 seconds with the limits brought on by Python and the GPS module. Similarly, the BPI count rate is collected every 0.2 seconds and stored along with the GPS position and other relevant data.

3.3.3 Data Handling

The data handling portion of the code makes use of Savitzky-Golay data filtering and Bayesian statistics to reduce the impact of data spikes and to exclude area from the rest of the search.

Dr. Benjamin Magocs' Savitzky-Golay Data Filtering

The Savitzky-Golay data filtering method used in this project was designed by Dr. Lajos Magocs. The purpose of this method is to determine the filter window size based on the number of data points reported during the tier. This is done by setting the window size to be 71 if the length of the data list is greater than 71. If the length of the list is less than 71, the window size is equal to length of the data list divided by 3 and forced to be an odd number. Further, if the length of the data list is less than 20, the window size is set to 5. It utilizes a least squares method to smooth the data across the window. This method is designed to smooth the data to account for variation in the source and background counts. The ground station performs this data filtering once every drone sends a "C" status flag.

Bayesian Area Exclusion

This Bayesian Area Exclusion method is designed in such a way to terminate a tier early once a certain threshold has been found. This is done to exclude the rest of the tier search area thus reducing the time over a large area. This method works by having the package check the count rate against a hard-coded threshold value and flying back to the GPS coordinates associated with that count rate. Once the vehicle is hovering there, it begins to transmit a "1B" status flag to the ground station which prompts it to begin taking an average over 50 messages from the vehicle. If this average is higher or equal to the ground station Bayesian threshold value, then the ground station transmits a tier 2 and new initial data to the vehicle. If this average is less than the threshold, the vehicle continues to execute tier 1.

The package threshold value is determined by knowledge of the source and background and the furthest possible distance to the source in tier 1. Tier 1 has a maximum lateral distance at the corner of the search area. In the case of a tier 1 with 50 m spacing, this lateral distance is 35.35 m due to the 25 m padding from the edge of the search area. The distance between the detector in the air and the source is then the hypotenuse of a triangle with legs equal to the lateral distance and the altitude. For an altitude of 50 m and default tier 1 settings, this detector to source distance is equal to 61.23 m. With the simulated source described later in Chapter 4 Section 1 the source count will be equal to approximately 4 c/s and have a normally distributed background with a mean of 176 c/s and a standard deviation of 1.6 c/s. Using the value of the third standard deviation, 180 c/s, and the expected source counts the drone side Bayesian threshold value is set to 184 c/s to give a low false positive result. The ground station average threshold value is found by adding the expected source counts, 4 c/s, to the mean of the background, 176 c/s, to get a value of 180 c/s.

3.3.4 Tiers

The flight paths of the vehicles are broken up into three main sections called tiers. These tiers cover a different scale and detail. All tiers use a transverse method to search the area. Each tier takes the same initial data: a South Western most point, a width, a height, a spacing, and an altitude. These parameters are hard coded into the ground station main but are easily changed by the user and passed on to each vehicle over the radios. When a vehicle receives a tier's initial data, it begins to calculate a flight path based on Dr. Lajos Magocs' Vertical Grid function. This function has been modified to move the start position to the north and east by half of the spacing variable and reduce the width and height by the same factor of half of the spacing. This is done to provide the vehicle a safeguard against crashing into other vehicles or objects at the border as well as allow for non-overlapping detector windows. This function originally made use of the haversine equation and module but has been modified to use the geodesic library to allow for higher accuracy at all latitudes at the cost of a slightly higher calculation time. As the number of the tier increases, the search area covered and distance between path laps decrease. This allows for the accuracy of the system to increase as one allows it to run. The starting direction of travel is determined by comparing the width and height, and determining the longest side and traveling in that direction first.

Tier 1

Tier 1 is a transverse pattern over the largest search area. This is the only tier to make use of Bayesian area exclusion and potentially multiple drones. This tier splits up the search area by "N" number of drones and the areas and start point for each drone is calculated by the ground station and transmitted to each vehicle. This tier's calculations begin when the ground station transmits the initial tier data while the vehicle is on the ground. Once the vehicle has received this data it begins to calculate the flight way points and determines if it is armable. When the way point calculations are finished and the arm checks are performed, the vehicle broadcasts a "R" for ready status flag which prompts the user to hit "Enter" on the ground station to launch the vehicle by transmitting a "T" command flag. This command flag is echoed in the vehicle's status flag as it takes off to the desired altitude. Once this altitude has been achieved the status flag changes to "F1" for flying to tier 1. Once the vehicle has reached the South West corner, its status flag is "1" and continues till the end of the list of way points or the Bayesian threshold is met. Tier 1 as currently implemented covers a 1 km x 1 km search area. This tier's spacing and altitude are both 50 m. As each drone ends its search area it begins to transmit a "1C" to the ground station in order to let it proceed with the Savitzky-Golay data filtering and calculating the tier 1 estimated source position.

Tier 2

Tier 2 is a transverse pattern over the middle search area. This tier does not make use of Bayesian area exclusion or multiple drones. This tier starts when the ground station has calculated the tier 1 estimated source position and the new South West corner of tier 2's search area. The ground station then identifies the vehicle with the highest battery life and transmits the tier 2 initial data to it. While the vehicle is hovering and receiving the tier 2 initial data, it calculates the tier 2 movement way points. When this calculation is done, the vehicle begins to move to the South West corner while broadcasting a "F2" status flag. Once at South West corner, the status flag becomes "2" for the rest of the tier. At the end of the tier 2 list of way points, the vehicle hovers and transmits "2C" status flags.

Tier 3

Tier 3 is a transverse pattern over the smallest search area. This tier differs from the other two in that it calculates intermediate points at which to hover for a preset amount of time. These intermediate points are equally spaced 5 m away from one another. This tier begins similarly to tier 2 as the ground station must calculate the estimated source position from tier 2 and the new South West corner. This corner and the initial data of a 30 m width, 30 m height, 5 m spacing, and 50 m altitude are transmitted to the vehicle. After receiving this initial data, the vehicle continues to hover till it has completed its flight way point calculations and begins to move towards the corner. As it moves towards the corner it broadcasts a "F3" status flag till it reaches the corner and updates to a "3" status flag. As the vehicle approaches the intermediate way points it slows down to hover for a preset 10 seconds. After this time is complete, the vehicle continues to the next point till the end of the list when it transmits a "3C" status flag which allows the ground station to calculate the tier 3 estimated source position. After this point, the vehicle flies home transmitting a "FL" status flag till it reaches the launching location when its transmits a "L" status flag indicating to the operator that it is ready to be landed manually.

3.3.5 System Flow Chart

This section presents a combined look at both sides of communications and the tier code and is presented in a full system flow chart below in Appendix C Figures C.3, C.4, and C.5. These flow charts demonstrate how the command and status flags are used in the context of running the system. The drone column represents single or multiple vehicles and the ground station column will describe with which vehicle it is communicating. After the vehicle arrives at the home location and is manually taken over, the Python script loses control and the drone will de-arm when landed.

Chapter 4

Experimental Plan

There are two parts to the simulations used to test this system: fully simulated and bench-top testing. The fully simulated tests are done using the same functions as the full flight code but executes exclusively on one computer without having to transmit over radio. This setup also allows the user to change the data collection and processing methods and the source position and strength easily. Thew fully simulated testing was mainly to experiment with 2D Savitzky-Golay, binning data, and equally distributed data collection points. The bench top testing is a full execution of the complete code but without a connection to the Pixhawk flight computer. This means the code runs on the package's Raspberry Pi, receives, and transmits over the Xbee radios, and is powered by the batteries. Due to the lack of connection to a Pixhawk flight computer, Dronekit software in the loop (SITL), Mavproxy, and ArduPilot Mission Planner must be used to simulate the drone. This method also requires the use of a simulated source and background. The bench top testing method is the primary focus for testing this system as it makes use of the hardware as much as possible without requiring an actual flight.

4.1 Simulations

As previously stated, the primary method of testing this system is doing bench top testing using all the hardware except for the actual drone. To simulate the drone, Dronekit software in the loop is employed. The SITL drone is not user configurable thus some factors of the

HSE HL-20 are not accurately modeled. These factors are maximum speed, acceleration, GPS accuracy, wind conditions, and battery life. Beyond the drone, a simulated source and background are calculated. The simulated source is a 10 mCi Cesium-137 source which emits a 662 keV gamma particle. This simulated source accounts for the shielding done by the air between the vehicle and source position as well as the geometric and intrinsic efficiency of the EJ-276 plastic scintillator crystal. The geometric efficiency is calculated by the ratio of areas approximation using the side rectangular area of the right cylinder plastic scintillator and the surface area of a sphere of radius equal to the distance between source and vehicle. The intrinsic efficiency used is 35 % and was provided by a manufacturer handbook for crystal thicknesses of 50mm.

$$I(r) = I_0 * e^{-\mu * r} = 3.7 * 10^7 * e^{-9.35*10^{-5}*r} \tag{4.1}$$

$$\epsilon_{geo} = A_d/(4 * \pi * r^2) = (2 * 2.54 * 2 * 2.54)/(4 * \pi * r^2) \tag{4.2}$$

$$\epsilon_{int} = 0.35 \tag{4.3}$$

$$Counts_{Source} = \epsilon_{int} * \epsilon_{geo} * I * e^{-\mu * r} \tag{4.4}$$

The background count rate is modelled by a normal distribution with a mean of 176 c/s and a standard deviation of 1.6 c/s. This is then added to the source counts to simulate the total count rate in the detector.

4.1.1 Testing Criteria

Testing this system requires multiple complete simulations using differing testing criteria. The testing criteria are Bayesian area exclusion, the number of drones, altitude, source position, and source strength. Bayesian area exclusion can either be enabled or disabled. The number of drones can vary between a single drone, or two drones. The altitude of the drone has been varied between 25 m, 50 m, and 75 m. The source position is also varied between three position: centered, centered North edge, and North West corner. The source strength is also varied between 0.1 mCi, 10 mCi, and 1000 mCi and the altitudes required for those differing source strengths to achieve positional error comparable to 10 mCi at 50 m altitude.

Chapter 5

Results

5.1 Bayesian Test

The Bayesians tests check to ensure the area exclusion method works as intended. The Bayesian area exclusion method cancels the remaining tier 1 way points if the threshold and average are met and continues to tier 2 centered about the point associated with the threshold value.

5.1.1 Threshold Not Met

The Bayesian disabled test made use of a single simulated vehicle. The source was 500 m north and 500 m east of the south west corner. The source activity was 10 mCi. The vehicle's target altitude was 50 m. As shown below in the flight path map, the source was equally spaced between two laps of the flight path. With this source positioning and altitude, the detector count has a good chance of being higher than Bayesian threshold but was intentionally disabled to perform this test. For this test the relevant figures are in Appendix D Figure D.1 and D.2 and data is recorded in Table D.1.

5.1.2 Threshold Met

This test made use of a single simulated vehicle. The source was 500 m north and 500 m east of the south west corner. The source activity was 10 mCi. The vehicle's target altitude was 50 m. As shown below in the flight path map, the source was located just off the flight path. With this source positioning and altitude, the detector count has a good chance of being higher than Bayesian threshold and passed the threshold of 184 c/s and average of 176 c/s. As a result of passing the Bayesian threshold, the remainder of tier 1 was negated, and the vehicle continued to tier 2 at slightly lower accuracy. For this test the relevant figures are in Appendix D Figure D.3 and D.4 and data is recorded in Table D.2. The comparison between the two Bayesian tests is in Appendix D Table D.3.

5.2 Number of Drones

These tests check to ensure that multiple drones are capable of reporting back to the same ground station and measure the time reduction from the number of drones. This time reduction should not be precisely half of a single drone tier 1 time but instead slightly longer since the second drone has to wait for the first to take off and clear the area before it travels to its search area.

5.2.1 Two Drones

This test makes use of two drones and a centered 10 mCi Cs-137 source. The source position is 500 m north and 500 m east of the south west corner of the search area. The altitude for this flight test was 50 m. The flight paths should closely replicate the single drone result with extensions from the second drone's "F1" portion of its flight. This test is the baseline test from which all other tests vary.For this test the relevant figures are in Appendix D Figure D.5 and D.6 and data is recorded in Appendix D Table D.4. The comparison between the single and two drones tests is in Appendix D Table D.5.

5.3 Altitude

The altitude tests are designed to determine the system accuracy as altitude is changed from the default 50 m. For these tests, the Bayesian thresholds are disabled to achieve consistent results. The altitude will be change to 25 m and 75 m from the baseline of 50 m. The accuracy would be expected to increase as the vehicle decreases in altitude due to the increase in the ratio of expected source counts to the background counts. The opposite should be true for increasing altitude meaning that the accuracy of the system should decrease.

5.3.1 25 m Altitude

The 25 m altitude test is like the two drone 50 m altitude with a centered 10 mCi Cs-137 source but with a lower target altitude. The source is in the same position 500 m north and 500 m east of the south west corner of the search area. For this test the relevant figures are in Appendix D Figure D.7 and D.8 and data is recorded in Appendix D Table D.6.

5.3.2 75 m Altitude

The 75 m altitude test is similar to the two drone 50 m altitude with a centered 10 mCi Cs-137 source but with a higher target altitude. The source is in the same position 500 m north and 500 m east of the south west corner of the search area. For this test the relevant figures are in Appendix D Figure D.9 and D.10 and data is recorded in Appendix D Table D.7. The comparison between the differing altitude tests is in Appendix D Table D.8.

5.4 Source Position

The source position tests are designed to evaluate the system accuracy as the source location is changed from the centered position baseline. For these tests, the Bayesian thresholds are disabled to achieve consistent results. The two tests conducted to check this aspect of the system are a source position in the north east corner and centered along the north edge. Checking the resilience against missing or reduced of information about the source is a significant aspect of the tests. These cases are the furthest possible distances between the source and detector.

5.4.1 North East Corner Source

The North East Corner source test is similar to the two drone 50 m altitude with a centered 10 mCi Cs-137 source but the simulated source has been moved to the north east corner of the search area. The precise positioning of the source is 1000 m north and 0 m to the east of the south west corner. For this test the relevant figures are in Appendix D Figure D.11 and D.12 and data is recorded in Appendix D Table D.9.

5.4.2 Centered Northern Edge Source

The Centered North Edge test is similar to the two drone 50 m altitude with a centered 10 mCi Cs-137 source but the simulated source has been moved to a centered position on the north edge. The precise positioning of the source is 1000 m north and 500 m to the east of the south west corner. For this test the relevant figures are in Appendix D Figure D.13 and D.14 and data is recorded in Appendix D Table D.10. Source Position test comparison is in Appendix D Table D.11.

5.5 Source Strength

The source strength tests are designed to analyze the system accuracy as the source strength is raised and lowered from the baseline of 10 mCi. For these tests, the Bayesian thresholds are disabled to achieve consistent results. The two tests conducted to check this aspect of the system are a source strength of 0.1 mCi and 1000 mCi. Testing against high and low ratios of source counts to background counts is significant as the source counts can be hidden by variation in the background counts. For both the low and high source strengths altitude is first run at the baseline 50 m altitude and then varied till the system accuracy is in the same range as the 10 mCi source at 50 m.

5.5.1 0.1 mCi

The smaller source test makes use of a centered Cs-137 source with a strength of 0.1 mCi. Initially this test was performed at 50 m but returned unsatisfactory results. The source count rate was expected to be 0.05 c/s which is significantly below the variation in the background. The 50 m flight test is shown in Appendix D Figures D.15 and D.16 and the flight data is show in Table D.12. As a result of the low accuracy at 50 m altitudes, the altitude was dropped to 25 m and the test repeated. These results while better were still inadequate and the improvement was due to lucky statistics as the expected count rate was 0.15 c/s which is still significantly below the variation in the background counts. The 25 m flight test is shown in Appendix D Figure D.17 and D.18 and the flight data is show in Table D.13. To achieve source count rates similar to the 10 mCi at a 50 m altitude (4.04 c/s), the search pattern had to be tighten to 5 m spacing for all tiers and the altitude dropped to 6.75m as these values create a distance of 7.8 m between source and detector. To save time on the simulation the search area was reduced from 1 km x 1 km to 200 m x 200 m with the source at 100 m north and 100 east of the south west corner which does not significantly alter the accuracy. Along with this reduction in scale, the number of drones was reduced from two to a single drone. The 6.75 m flight test is shown in Appendix D Figures D.19 and D.20 and the flight data is show in Table D.14. The comparison between all 0.1 mCi sources tests is found in Appendix D Table D.15.

5.5.2 1000 mCi

The larger source test makes use of a centered Cs-137 source with a strength of 1000 mCi. Initially this test was performed at 50 m and achieved satisfactory results. The source count rate was expected to be 1565 c/s which is significantly higher than the variation in the background. The 50 m 1000 mCi test flight path is shown in Appendix D Figures D.21 and D.22 with the flight data being recorded in Appendix D Table D.16. As a result of the high accuracy at 50 m altitudes, the altitude was increased to 248 m and the test repeated. This altitude was determined by finding the straight-line distance between detector and source that gave an expected source count rate near 4.04 c/s. The 248 m 1000 mCi test flight path is shown in Appendix D Figures D.23 and D.24 with the flight data being recorded in Table D.17. The comparison between the 50 m and 248 m tests is shown in Appendix D Table D.18.

Chapter 6

Discussion

6.1 2D Savitzky-Golay and Binning Methods

At the beginning of testing, many features were added in efforts to get higher accuracy more consistently. It was noticed that Savitzky-Golay data filtering has a strong preference for evenly spaced and distributed data points. This was commonly seen as there is more pull to the edge of the map where the vehicle slows down as it approaches a way point and collects more points do the constantly set rate. 2D Savitzky-Golay Filtering, 2D data binning and evenly space, and distributed measurement points were explored as a potential solution to this problem. In fully simulated tests, this method produced excellent results with an average error of less than 2.5 m using 1 m x 1 m bins for all possible source positions in the search area. Bins outside of the flight path were filled with the lowest recorded bin value as an assumption that it would be closest to background.

Implementing 2D data filtering, data binning, and using hardware proved to be more difficult. Attempts were made using many methods of binning attempted such as: binning by distance on the drone side of the system and binning by distance on the ground station. Binning on the drone side did not work as the velocity and position of the vehicle were always changing and proved difficult to track between the various threads. Commonly the vehicle would skip a measurement way point which would crash the system and prevent the drone from continuing its path. Binning on the ground station was the more practical of methods as the drone would have a constant high poll rate which should have guaranteed a measurement reported inside of the bin. Running with these settings using hardware over the 1 km x 1 km test area proved the same issue existed but with a lower probability of occurrence. This can be attributed to the GPS error in the simulated drone vehicle and relatively small bin sizes. This was commonly seen in the original tier 3 method which made use of a transverse path with measurement points every 1 m which were then binned into 1 m x 1 m bins. During this testing, the drone frequently had division by zero errors as the vehicle's GPS error caused crossing flight paths and thus no values in the bin. The measurement way points and bins were then increased to every 5 m and 5 m x 5 m bins and the issue decreased in occurrence but was still persistent. When the binning method worked, it was prone to taking 15-20 minutes of calculation time after a 1 km x 1 km tier 1 test. As a radical simplification method, binning was removed and hovering at each way point was implemented. This system removed the errors associated with binning and division by zero and 2D Savitzky-Golay was reverted to 1D. These changes caused a potentially less accurate but more reliable system.

6.2 Drone Communications

The hardware testing of this system makes use of the UDP protocol over the 900 MHz radios and Wi-Fi. This method was used for both communications between the Raspberry Pi drone program and ground station program over the radios as well as the Raspberry Pi drone program to the simulated Pixhawk and drone on the ground station over Wi-Fi. For the radio UDP communications, dropped packets are not a potential problem as both Raspberry Pi and ground station are programmed to continue to send their respective messages until the other responds. For the communications over Wi-Fi, this became a significant problem as both ends have an unknown short timeout value which causes the drone Python script to disconnect and the simulated drone to stop receiving orders. As a result of not receiving any orders, the simulated drone then proceeds to lose altitude until it "hits the ground" preventing the recovery of the system. Thus, if either end of the system loses connection for a brief period, the system crashes and the simulation is invalidated and cannot continue. It is unknown what caused this timeout over the University of Tennessee's

Wi-Fi connection, but it happened frequently and at various points throughout simulations. Moving the system to real world testing connected to a physical Pixhawk and drone would theoretically reduce the chances of this error occurring significantly as the connection would be over a USB cable using UDP and should be more robust.

6.3 Bayesian Area Exclusion

For the Bayesian Area Exclusion tests, the primary concern is the time reduction effect of negating a portion of the tier 1 search area if the Bayesian threshold test is passed. The Bayesian Area Exclusion method occurs when two tests are passed, a single drone threshold and a ground station average value threshold. The drone threshold is passed when the drone reads a count rate higher than 184 c/s. The ground station threshold is an average of the count rates above the location the drone records the 184 c/s and is set slightly lower at 178 c/s. The ground station average threshold is calculated using 50 status messages from the vehicle. The vehicle sends these messages at a rate of 5 messages per second. If these two tests are passed, then the remaining search area is skipped, and the ground station begins tier 2 centered around the location at which the drone detected the threshold point. In the experimental case, the source is in the center of the search area and thus it is expected to pass the Bayesian threshold test after searching approximately half of the search area. For the simulation that passed these Bayesian tests, the drone found the threshold count rate when it was approaching the source. Therefore, this simulation run negated over half of the search area. This had the effect of reducing the tier 1 search time by 51% compared to a simulation run where the Bayesian test never triggered. The secondary result of the Bayesian tests is the tier 1 estimated source position accuracy. In this experimental case, the tier 1 estimated source position was 37.34 m away from the source location compared to the non-Bayesian test with a source estimate 24.8 m away. The Bayesian estimated source position is still within the tier 2 search area and allowed tier 2 and tier 3 to localize the source with acceptable accuracy.

6.4 Number of Drones

The number of drones test is primarily concerned with time reduction effects of using single or multiple vehicles. Since the search area is split equally between the number of vehicles, one would expect the tier search time to reduce by the number of vehicles as well. This is good for an estimate, but any additional drone must wait for the first drone to clear the launch area before takeoff and fly to its starting point. As noted in the simulation the percent difference between the single drone and two drones tier 1 is -46.97% which is close to what one would expect. The time reduction would get closer and closer to the single drone tier 1 time divided by the number of drones as the search area decreases as there is less travel time for all vehicles.

6.5 Altitude

The altitude tests, determines the accuracy of the package as the altitude of the vehicles changes. The altitude was varied from 50 m to 25 m and 75 m. It is expected that the lower the altitude will increase the source count rates and thus have a greater potential to be higher than the variation in the background. The opposite should be true as altitude increases. This is seen in the test results. When comparing the 50 m control case to the 25 m, the percent difference for tiers 1 and 2 were very similar at 0.57% and 0.54% while the tier 3 accuracy improved by 35.63%. This can also be seen in the 75 m test where the percent difference from the control was considerably higher for tier 2 and 3 at 203.57 % and 185 % while tier 1 maintained the similar accuracy of -1.62%. The altitude change tests performed as expected and, while the 75 m percentage difference was high, it was only an order of magnitude higher.

6.6 Source Position

The source position tests are primarily concerned with verifying that the system can identify a source in test cases that have been noted to be trouble cases in the fully simulated tests. These positions are edges and corners of the search area. These cases are difficult to identify as the system collects approximately half and a quarter of the radiation count field. For the north west corner case, the percent differences were fairly large at 40.18%, -0.27%, and 109% for tiers 1, 2, and 3. For the centered north edge case, the percent differences were still high but not as high as the corner case as shown by the 27.61%, -0.46%, and 104.38% for each tier respectively. Despite the relatively high percent differences, the errors are close together and are within the same order of magnitude.

6.7 Variable Source Strengths

The variable source strengths tests are concerned with ability to detect the source and the settings changes needed as the source strength varies. The changes to the settings for a test are in effort to achieve accuracy like the baseline two drone 50 m altitude, and 10 mCi source test.

6.7.1 0.1 mCi Source

For the 0.1 mCi source test, it is expected that the altitude will need to be reduced and possibly reducing the spacing. For the 25 m and 50 m tests the tier codes remained consistent with the control case. For the 6.75 m test, spacing for all tiers have been reduced to 5 m to achieve source counts greater than the variation in the background. For the 50 m case, the percent differences are 2228.23%, 11899.94%, and 13210.16% for tier 1 - 3. This inaccuracy is most likely due to the source counts at this altitude being significantly lower than the variation in the background and thus the system is picking a random hot pot from background. Similar but lesser results are seen in the 25 m test, with this tests percent differences being 522.55%, 2688.45%, and 3103.14%. This test's error stems from the same cause as the 50 m test but a hot spot was generated considerably closer to the source position.

6.7.2 1000 mCi Source

For the 1000 mCi source tests, it is expected that altitude can be increased without a massive increase in error. The test altitudes used are 50 m and 248 m. This 248 m altitude is calculated finding the highest altitude that produces a source count rate of greater than 4 c/s. The 50 m test produced percent differences of -0.79%, -20%, and -57.52%. The 50 m test produced significantly more accurate results as the source counts are significantly higher than the variation in the background. For the 248 m test, the percent differences are 51.31%, 616%, and 566.45%. The raw errors for this test are within one order of magnitude and still fairly accurate at a max of 39.4 m.

Chapter 7

Conclusion

This SWARM system seems to perform acceptably within the design constraints. The Bayesian area exclusion method is configurable to a source strength and altitude and acceptable false positive and inaccuracy tolerances. As currently configured, the system reduced the time for the tier 1 search by 51% and did not produce an error large enough to be outside of tier 2.

The system also behaved as expected when used with single and multiple drones. The increase in the number of drones followed loosely a formula of the single drone tier 1 search time divided by the number of drones. This test also did not significantly increase or decrease source estimate error.

The system behaved as expected with changes in altitude. The lower the altitude the greater the estimate accuracy and a higher altitude will decrease the estimate accuracy. This is seen in the 25 m and 75 m tests when compared to a 50 m control. The accuracy increases when the altitude is reduced from 50 m to 25 m by about 35%. For the 75 m test, the accuracy decreased by a maximum of 203% but the final tier was only off by 13.3 m.

The system was tested against difficult source positions such as the corner and an edge case. For the corner case, the error increased by 109.52% which translates to a 9.8 m error. For the edge case, the error increase was slightly lower at 104.4% which equated to a 9.55 m error. These errors are still within tolerance of the system.

This system was also tested against a source 100 times stronger and a source 100 times weaker than the control 10 mCi. These source activities were 0.1 mCi and 1000 mCi. For the 0.1 mCi test, the altitude had to be decreased from 50 m to 25 m to 6.75 m. For the 6.75 m test, the spacing for all tiers was also set to 5 m. For the 50 m and 25 m tests, the system was wildly inaccurate with error distances greater than 100 m. This was due to the source count rates being statistically insignificant to the background. For the 6.75 m test with reduced spacing, the expected counts should be like the 10 mCi test at 50 m. This method had errors very similar if not better than the control case with the final estimate being 3.16 m from the source location. For the 1000 mCi test, the altitudes were maintained at 50 m and increased to 248 to achieve similar count rates to the 50 m altitude and 10 mCi case. For the 50 m case the error was significantly lower at a final estimate error of 1.98 m. For the 248 m case, the error was increased by a maximum of 616.54% but this only equated to a final error of 31.15 m.

Overall, the system performed well when tested against differing source positions and source strengths. The system also handled the altitude tests as expected with greater accuracy for the lower altitude simulation and only a slight decrease in accuracy for the higher altitude simulation. The Bayesian area exclusion method also performed well reducing the necessary flight time and not having significantly higher error in the tier 1 estimated source position.

Chapter 8

Future Work

There is much work to be done on this project, primarily real life testing on the system in the field. Testing in the field would eliminate the simulation errors. This would solve the errors with the dropping UDP communication packets over Wi-Fi and replace the Wi-Fi connection with a USB cable, which should be more consistent. When moving to a physical drone, the GPS accuracy has the potential to be greater than the GPS accuracy in the SITL simulated drone. This would potentially allow the user to implement the equally spaced points, data binning, and 2D Savitzky-Golay data filtering. Implementing these features would greatly increase the overall system accuracy as well as reduce the system maximum error. The system could also be tested against different sources of differing particle types and energies. Potentially different detector models could be swapped in and increase the quantity of counts collected and thus increase the accuracy at higher altitudes.

Bibliography

1 R. Pavlovsky et al., “3-D Radiation Mapping in Real-Time with the Localization and Mapping Platform LAMP from Unmanned Aerial Systems and Man-Portable Configurations,” arXiv:1901.05038 [physics], Dec. 2018, Accessed: Jan. 29, 2020. [Online]. Available: http://arxiv.org/abs/1901.05038.

2 P. G. Martin et al., “3D unmanned aerial vehicle radiation mapping for assessing contaminant distribution and mobility,” International Journal of Applied Earth Observation and Geoinformation, vol. 52, pp. 12–19, Oct. 2016, doi: 10.1016/j.jag.2016.05.007.

3 R. B. Wilkerson, “A Bayesian Approach to Aerial Localization of Radioactive Sources,” p. 60.

4 S. J. Willmon, “A Bayesian Approach to Broad-Area Nuclear and Radiological Search Operations,” p. 107.

5 J. Jiang et al., “A prototype of aerial radiation monitoring system using an unmanned helicopter mounting a GAGG scintillator Compton camera,” Journal of Nuclear Science and Technology, vol. 53, no. 7, pp. 1067–1075, Jul. 2016, doi: 10.1080/00223131.2015.1089796.

6 “Aerial Measuring System (AMS),” Energy.gov. https://www.energy.gov/nnsa/aerial-measuring-system-ams (accessed Nov. 14, 2021).

7 C. Lyons and D. Colton, “Aerial Measuring System in Japan,” Health Physics, vol. 102, no. 5, pp. 509–515, May 2012, doi: 10.1097/HP.0b013e31824d0056.

8 Y. Sanada and T. Torii, “Aerial radiation monitoring around the Fukushima Daiichi nuclear power plant using an unmanned helicopter,” Journal of Environmental Radioactivity, vol. 139, pp. 294–299, Jan. 2015, doi: 10.1016/j.jenvrad.2014.06.027.

9 D. Connor, P. G. Martin, and T. B. Scott, “Airborne radiation mapping: overview and application of current and future aerial systems,” International Journal of Remote Sensing, vol. 37, no. 24, pp. 5953–5987, Dec. 2016, doi: 10.1080/01431161.2016.1252474.

10 Jérôme Renard, “compass bearing between two points in Python,” Gist. https://gist.github.com/jeromer/2005586 (accessed Dec. 10, 2020).

11 T. Lazna, P. Gabrlik, T. Jilek, and L. Zalud, “Cooperation between an unmanned aerial vehicle and an unmanned ground vehicle in highly accurate localization of gamma radiation hotspots,” International Journal of Advanced Robotic Systems, vol. 15, no. 1, p. 172988141775078, Jan. 2018, doi: 10.1177/1729881417750787.

12 “Delaunay Triangulation - an overview — ScienceDirect Topics.” https://www.sciencedirect.com/topics/earth-and-planetary-sciences/delaunay-triangulation (accessed Jan. 29, 2020).

13 K. Kurvinen, P. Smolander, R. Pöllänen, S. Kuukankorpi, M. Kettunen, and J. Lyytinen, “Design of a radiation surveillance unit for an unmanned aerial vehicle,” Journal of Environmental Radioactivity, vol. 81, no. 1, pp. 1–10, Jan. 2005, doi: 10.1016/j.jenvrad.2004.10.009.

14 J. Aleotti et al., “Detection of Nuclear Sources by UAV Teleoperation Using a Visuo-Haptic Augmented Reality Interface,” Sensors (Basel), vol. 17, no. 10, Sep. 2017, doi: 10.3390/s17102234.

15 “Drone options: the use of unmanned aerial vehicles for radiation monitoring came to the forefront after Fukushima, but they have applications beyond contamination assessment,” Nuclear Engineering International, vol. 60, no. 732, p. 40, Jul. 2015.

16 “efficiency-calculations.pdf.” Accessed: Dec. 11, 2020. [Online]. Available: https://www.crystals.saint-gobain.com/sites/imdf.crystals.com/files/documents/efficiency-calculations.pdf.

17 S. Mochizuki et al., “First demonstration of aerial gamma-ray imaging using drone for prompt radiation survey in Fukushima,” J. Inst., vol. 12, no. 11, pp. P11014–P11014, Nov. 2017, doi: 10.1088/1748-0221/12/11/P11014.

18 W. Czaja, B. Manning, L. McLean, and J. M. Murphy, “Fusion of aerial gamma-ray survey and remote sensing data for a deeper understanding of radionuclide fate after

radiological incidents: examples from the Fukushima Dai-Ichi response," J Radioanal Nucl Chem, vol. 307, no. 3, pp. 2397–2401, Mar. 2016, doi: 10.1007/s10967-015-4650-z.

19 G. Micconi, J. Aleotti, S. Caselli, G. Benassi, N. Zambelli, and A. Zappettini, "Haptic guided UAV for detection of radiation sources in outdoor environments," in 2015 Workshop on Research, Education and Development of Unmanned Aerial Systems (RED-UAS), Nov. 2015, pp. 265–271, doi: 10.1109/RED-UAS.2015.7441016.

20 K. Oyama, H. Wakabayashi, A. Takeuchi, and N. Ishitsuka, "Integration of 3D Trajectory Maps into a Local Distribution Map of Radiation Dose Using Unmanned Aerial Vehicle," in 2012 IEEE 36th Annual Computer Software and Applications Conference Workshops, Jul. 2012, pp. 607–612, doi: 10.1109/COMPSACW.2012.110.

21 P. G. Martin, O. D. Payton, J. S. Fardoulis, D. A. Richards, Y. Yamashiki, and T. B. Scott, "Low altitude unmanned aerial vehicle for characterising remediation effectiveness following the FDNPP accident," Journal of Environmental Radioactivity, vol. 151, pp. 58–63, Jan. 2016, doi: 10.1016/j.jenvrad.2015.09.007.

22 J. Han and Y. Chen, "Multiple UAV Formations for Cooperative Source Seeking and Contour Mapping of a Radiative Signal Field," J Intell Robot Syst, vol. 74, no. 1, pp. 323–332, Apr. 2014, doi: 10.1007/s10846-013-9897-4.

23 "NIST: X-Ray Mass Attenuation Coefficients - Air, Dry." https://physics.nist.gov/PhysRefData/XrayMassCoef/ComTab/air.html (accessed Dec. 11, 2020).

24 B. Magocs, "PADUA RADIOLOGICAL SEARCH SYSTEM," Doctoral Dissertations, Dec. 2019, [Online]. Available: https://trace.tennessee.edu/utk 7graddiss/5708.

25 M. Kazemeini, Z. Cook, J. Lee, A. Barzilov, and W. Yim, "Plug-and-play radiation sensor components for unmanned aerial system platform," J Radioanal Nucl Chem, vol. 318, no. 3, pp. 1797–1803, Dec. 2018, doi: 10.1007/s10967-018-6233-2.

26 R. P. Kelley, A. Enqvist, and K. A. Jordan, “Pulse shape discrimination in helium-4 scintillation detectors,” Nuclear Instruments and Methods in Physics Research Section A: Accelerators, Spectrometers, Detectors and Associated Equipment, vol. 830, pp. 44–52, Sep. 2016, doi: 10.1016/j.nima.2016.05.065.

27 F. Mascarich, T. Wilson, C. Papachristos, and K. Alexis, “Radiation Source Localization in GPS-Denied Environments Using Aerial Robots,” in 2018 IEEE International Conference on Robotics and Automation (ICRA), Brisbane, QLD, May 2018, pp. 6537–6544, doi: 10.1109/ICRA.2018.8460760.

28 R. Pöllänen et al., “Radiation surveillance using an unmanned aerial vehicle,” Applied Radiation and Isotopes, vol. 67, no. 2, pp. 340–344, Feb. 2009, doi: 10.1016/j.apradiso.2008.10.008.

29 L. L. I. Sharing (LLIS), “Radiological Assistance Program (RAP),” Homeland Security Digital Library, Jan. 01, 1969. https://www.hsdl.org/?abstractdid= (accessed Sep. 27, 2020).

30 P. Gabrlik and T. Lazna, “Simulation of Gamma Radiation Mapping Using an Unmanned Aerial System,” IFAC-PapersOnLine, vol. 51, no. 6, pp. 256–262, Jan. 2018, doi: 10.1016/j.ifacol.2018.07.163.

31 K. Oyama, K. Nakamura, H. Wakabayashi, A. Takeuchi, and N. Ishitsuka, “Situational map integration of dose distribution on the ground surface using Unmanned Aerial Vehicles,” in 2013 IEEE International Multi-Disciplinary Conference on Cognitive Methods in Situation Awareness and Decision Support (CogSIMA), Feb. 2013, pp. 171–174, doi: 10.1109/CogSIMA.2013.6523843.

32 P. G. Martin, O. D. Payton, J. S. Fardoulis, D. A. Richards, and T. B. Scott, “The use of unmanned aerial systems for the mapping of legacy uranium mines,” Journal of Environmental Radioactivity, vol. 143, pp. 135–140, May 2015, doi: 10.1016/j.jenvrad.2015.02.004.

33 V. Šmídl and R. Hofman, “Tracking of atmospheric release of pollution using unmanned aerial vehicles,” Atmospheric Environment, vol. 67, pp. 425–436, Mar. 2013, doi: 10.1016/j.atmosenv.2012.10.054.

34 P. Wasiolek, “U.S. Aerial Measuring System (AMS),” p. 19.

35 “Urethane.” https://webbook.nist.gov/cgi/cbook.cgi?ID=51-79-6 (accessed Nov. 29, 2020).

36 “Urethane Foam , Expanding Marine Polyurethane Foam.” http://www.uscomposites.com/foam .html (accessed Nov. 29, 2020).

37 B. Li, Y. Zhu, Z. Wang, C. Li, Z.-R. Peng, and L. Ge, “Use of Multi-Rotor Unmanned Aerial Vehicles for Radioactive Source Search,” Remote Sensing, vol. 10, no. 5, p. 728, May 2018, doi: 10.3390/rs10050728.

Appendices

Appendix A

Summary of Equations

A Chapter 4 Equations

Intensity Function

$$I(r) = I_0 * e^{-\mu * r} = 3.7 * 10^7 * e^{-9.35*10^{-5}*r} \tag{A.1}$$

Detector Geometric Efficiency Function

$$\epsilon_{geo} = A_d/(4 * \pi * r^2) = (2 * 2.54 * 2 * 2.54)/(4 * \pi * r^2) \tag{A.2}$$

Manufacturer's Intrinsic Efficiency for 50 mm Crystal

$$\epsilon_{int} = 0.35 \tag{A.3}$$

Simulated Source Counts as a Function of Linear Distance

$$Counts_{Source} = \epsilon_{int} * \epsilon_{geo} * I * e^{-\mu * r} \tag{A.4}$$

Appendix B

Chapter 2 Figures and Tables

A Radiation Survey and Dose Mapping

Table B.1: Survey Fixed-Wing

	AMS[34]	Design of a Radiation ... UAV[13]
Model of Vehicle	Beech King Air B-200	RUAG Ranger UAV
Class of Vehicle	Fixed Wing	Fixed Wing UAV
Engine	Twin Turbo Prop	2-cylinder 2 stroke engine
Mission Speed	72 m/s	67 m/s
Altitude Window	152.4 - 609.6 m	4500 m
maximum Endurance/Range	5 hrs/2100 km	9 hrs/180 km
maximum Payload	984 kg	45 kg

Table B.2: Survey Helicopters

	AMS[1]	Aerial Radiation ... Helicopter[2]
Model of Vehicle	Bell-412	Yamaha Motor Co. Rmaximum G1
Class of Vehicle	Helicopter	Unmanned Helicopter
Engine	Twin Pac Turboshaft	2 stroke 2 cylinder
Mission Speed	36 m/s	20 m/s
Altitude Window	15.24 -152.4 m	80 m
maximum Endurance/Range	3 hrs/670 km	1.5 hrs
maximum Payload	2040 kg	10 kg

[1] AMS[34]

[2] Aerial radiation monitoring around the Fukushima Dai-ichi nuclear power plant using an unmanned helicopter[8]

Table B.3: Survey Multi Rotors

	3D Unmanned ... and Mobility[3]	First ... in Fukushima[4]	Use of ... Source Search[5]	
Model of Vehicle	University of Bristol (UK) UAV	DJI S1000+	DJI Matrice 600	DJI Matrice 100
Class of Vehicle	Multi-Rotor UAV	Multi-Rotor UAV	Multi-Rotor UAV	Multi-Rotor UAV
Engine	LiPo powered	LiPo powered	LiPo powered	LiPo powered
Mission Speed	1 m/s	Uses a stationary method	1 m/s	1 m/s
Altitude Window	1-10 m	10-20 m	10 m	10 m
maximum Endurance	0.5 hrs	0.25 hrs	0.3 hrs	0.267 hrs
maximum Payload	5 kg	5 kg	5.5 kg	1.25 kg

[3] 3D unmanned aerial vehicle contaminant distribution and mobility[2]
[4] First demonstration prompt radiation survey in Fukushima[17]
[5] Use of Multi-Rotor UAVs for Radioactive Source Search[37]

Appendix C

Chapter 3 Figures and Tables

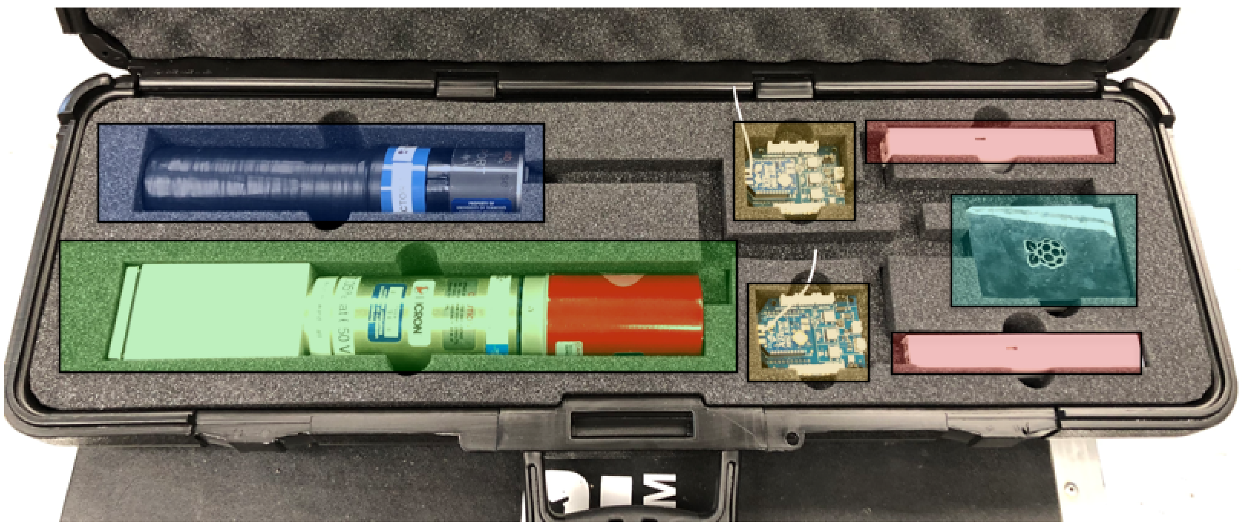

Figure C.1: Package Design with Components: Blue- EJ-276 BPI plastic scintillator for raw count rate collection and potentially gamma neutron discrimination; Green- NaI Osprey scintillator detector for potentially identifying isotopes; Yellow- Digi Xbee 900 MHz radios for communications between ground station and package; Red- 10,000 mAh batteries; Teal- Raspberry Pi for on board computing and data collection

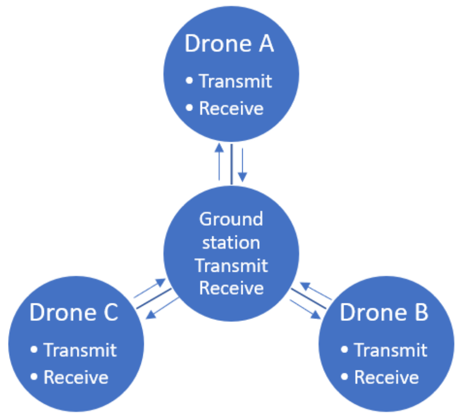

Figure C.2: High Level System Communications Diagram, arrows indicate information over 900 MHz radios, for more information see Figure 3.3

Table C.1: Command and Status Flag Definitions

Status Flag	Definition
I0/I	Initialization between the vehicle and ground station
R - Ready	Tier 1 flight path points generated, and the vehicle passes safety checks
T - Take off	Take off command and gaining altitude status
F1/2/3/L	Flying to the first point of Tier # or to home position
1/2/3	Flying through Tier # flight points
1B	Flying to/Hovering at Bayesian threshold point
-/+	Bayesian Test Boolean Fail/Pass
1C/2C/3C	Hovering after completing Tier #, waiting for next command
L	Hovering at home position after Tier completion

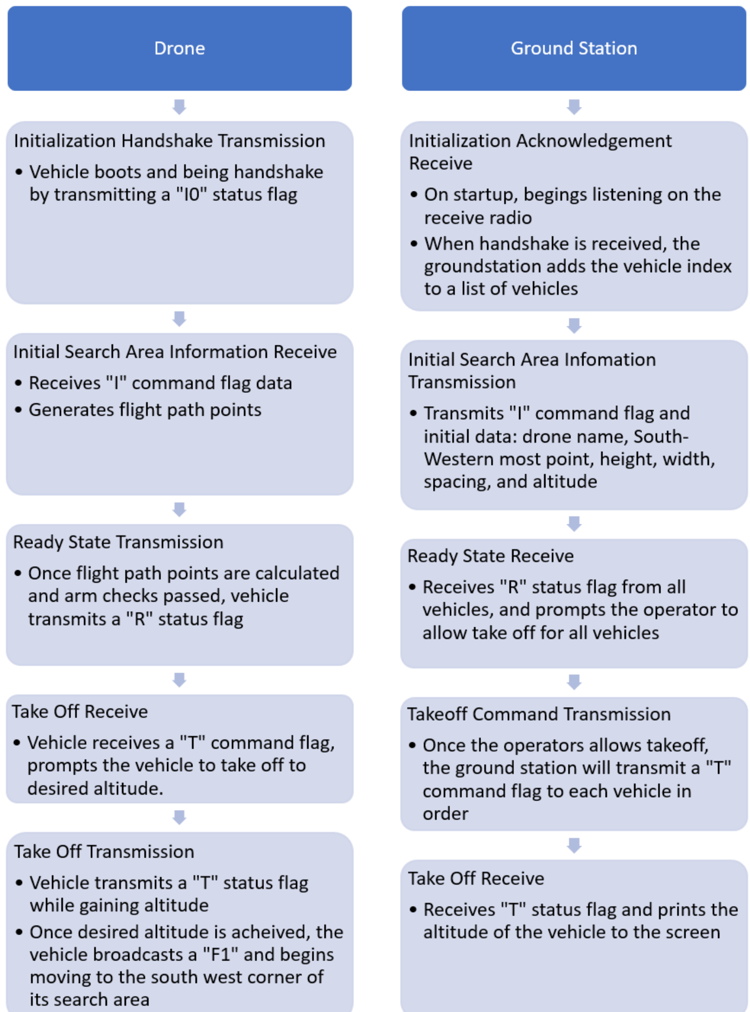

Figure C.3: Initialization and Take Off Communication Sequence

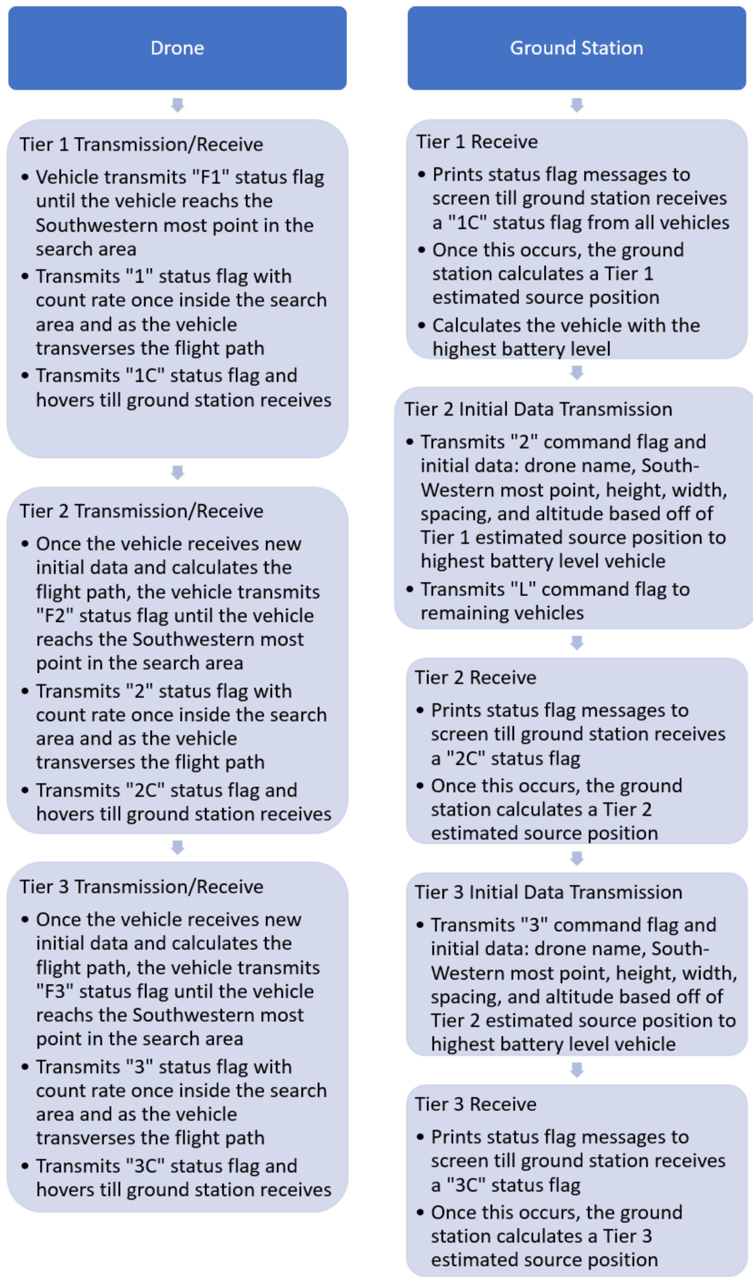

Figure C.4: Search Tier Communication Sequence

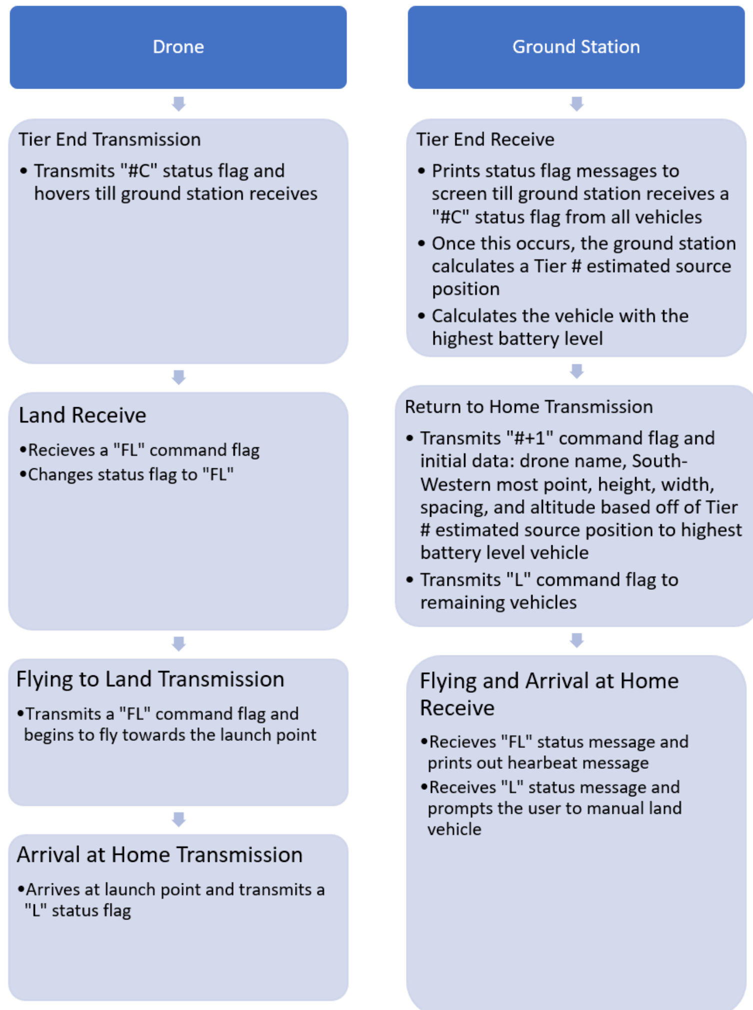

Figure C.5: Landing Communication Sequence

Appendix D

Chapter 5 Figures and Tables

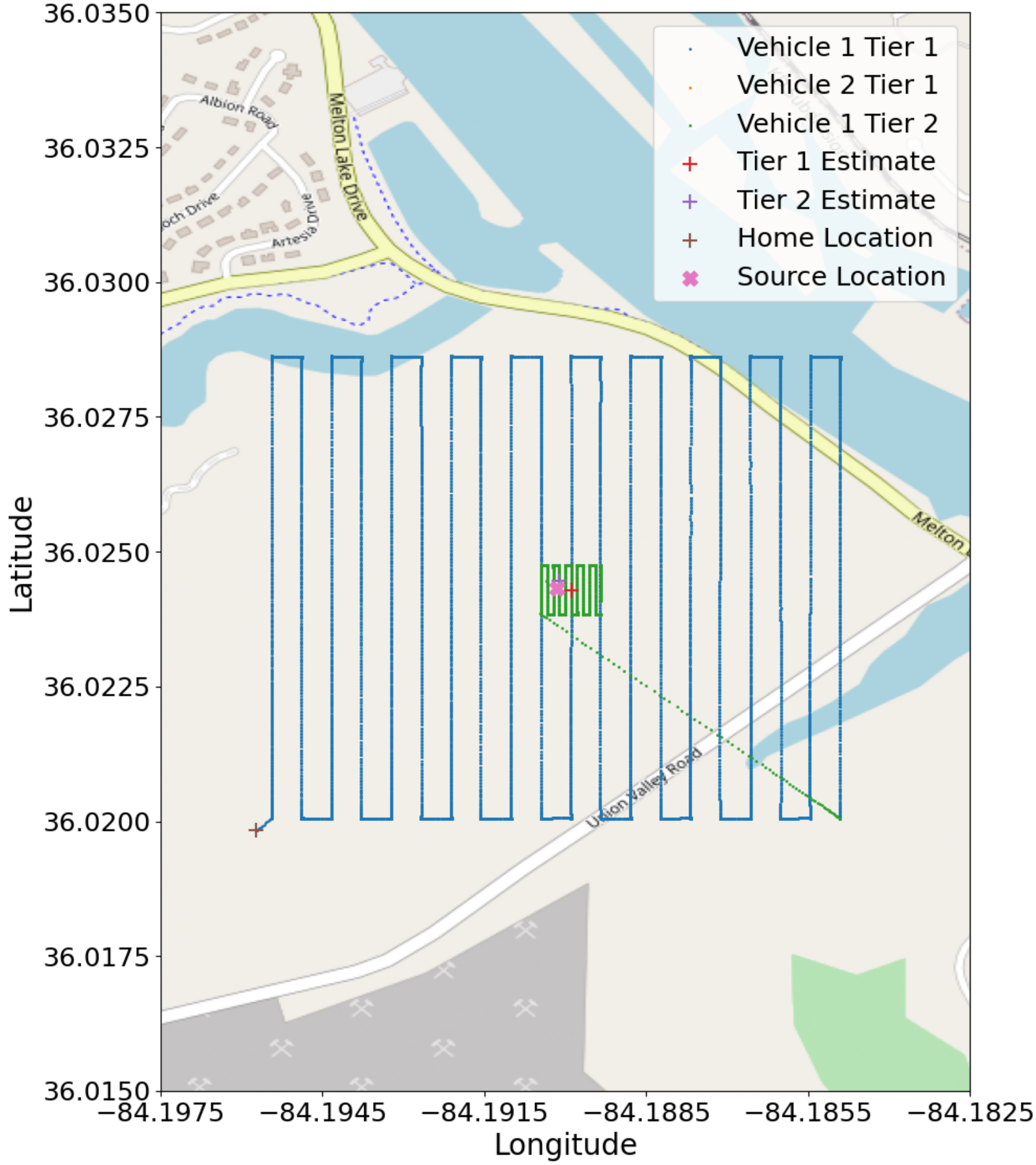

Figure D.1: Flight Path of Single Drone with Disabled Bayesian Threshold Method

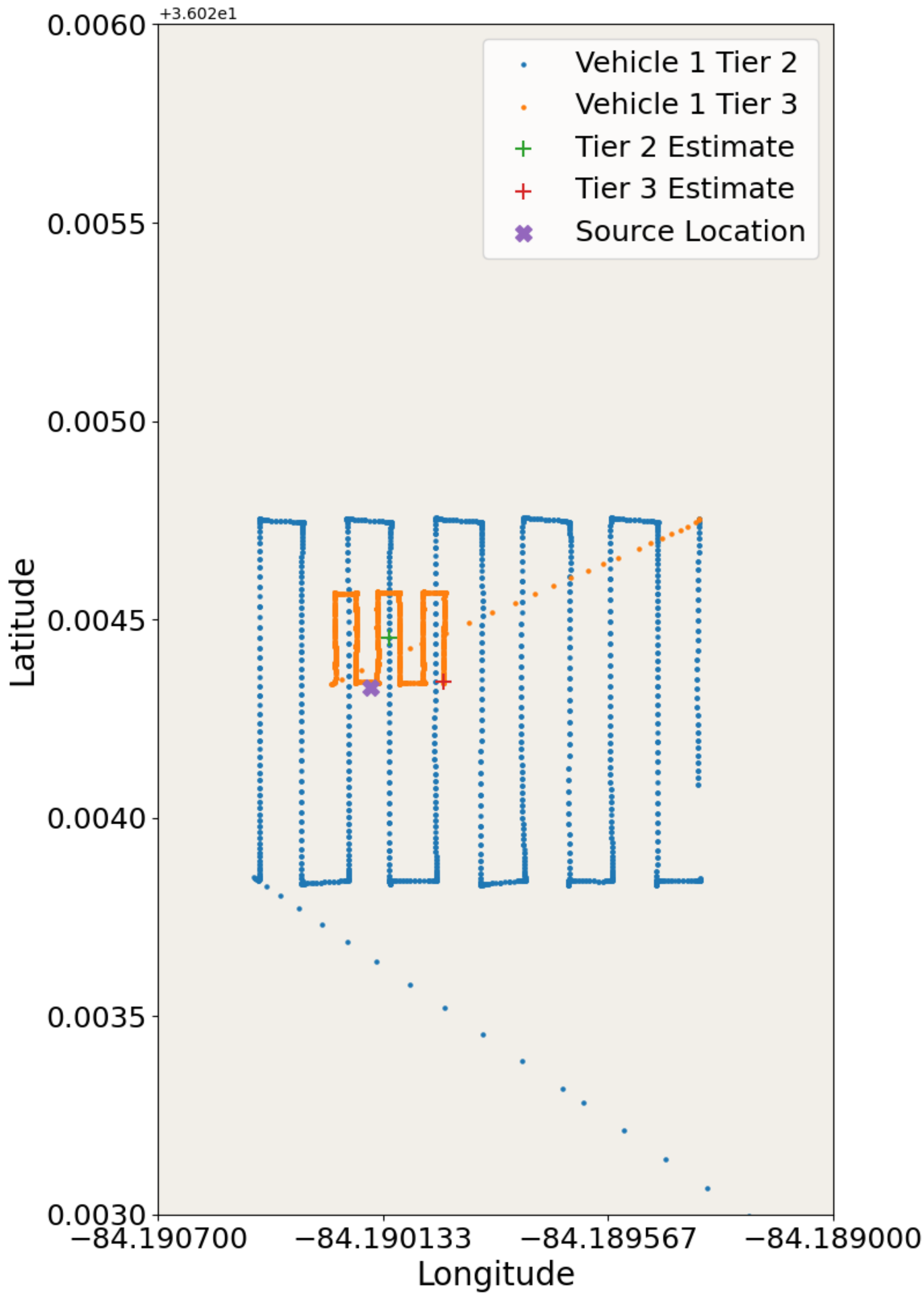

Figure D.2: Flight Path of Single Drone with Disabled Bayesian Threshold Method

Table D.1: Single Drone Bayesian Threshold Not Met

Title	Latitude	Longitude	Time(seconds)	Error Distance (m)
Source Location	36.0243282561	-84.1901636495		
Tier 1	36.0242943	-84.1898917	2704.58	24.8
Tier 2	36.0244552	-84.1901184	527.47	14.7
Tier 3	36.0243422	-84.1899811	646.30	16.5

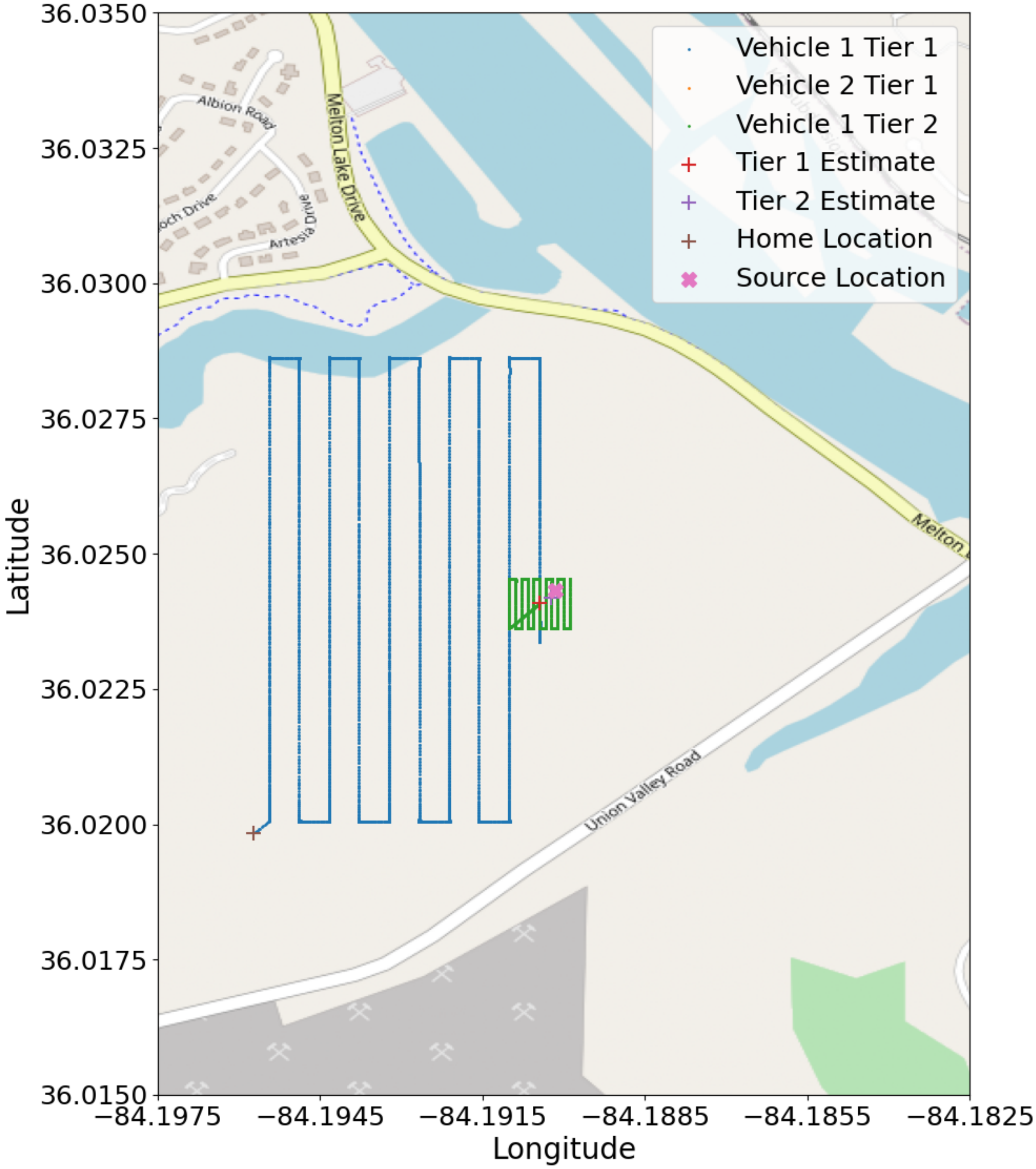

Figure D.3: Flight Path of Single Drone with passing Bayesian Threshold

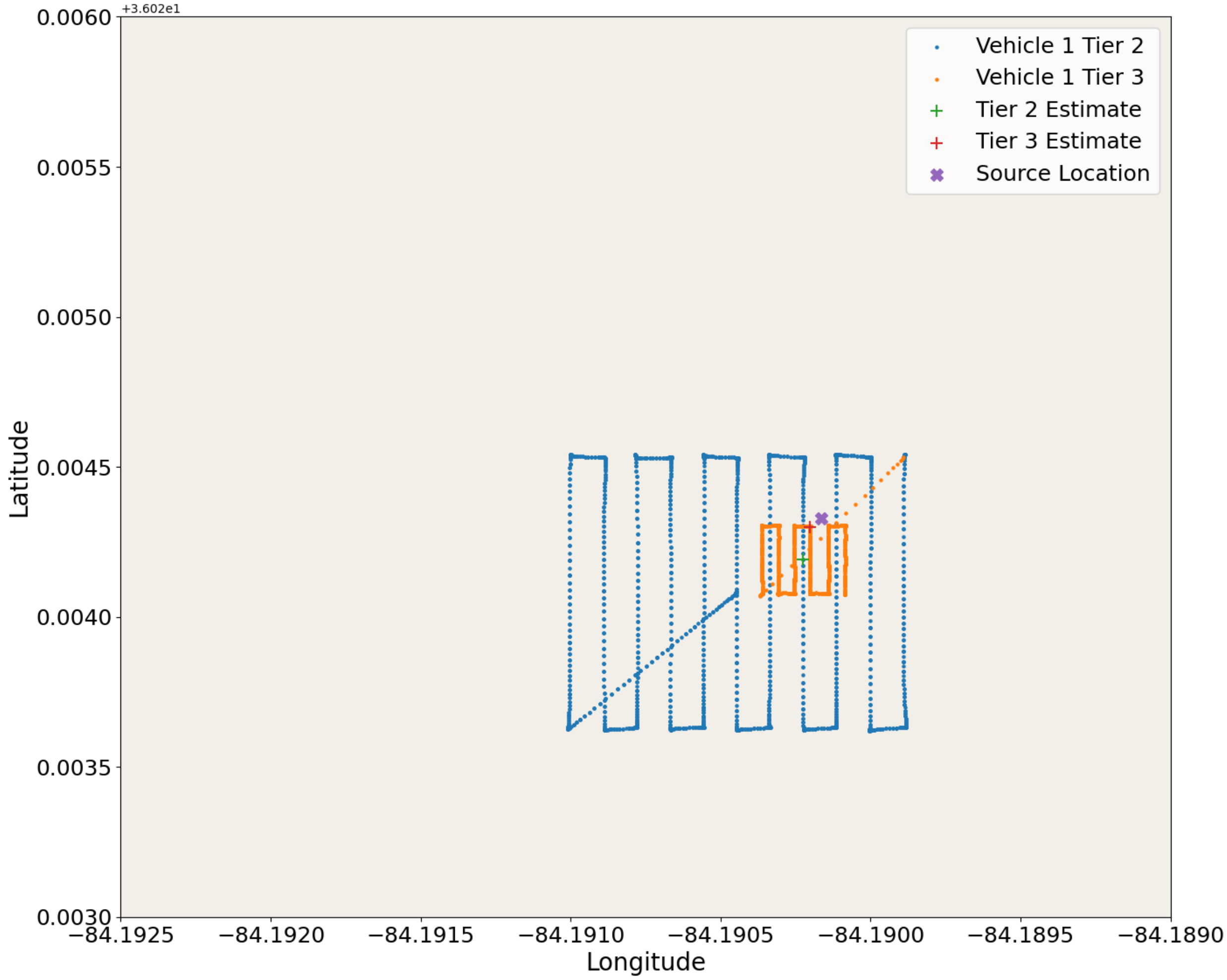

Figure D.4: Flight Path of Single Drone with passing Bayesian Threshold

Table D.2: Single Drone Bayesian Threshold Met

Title	Latitude	Longitude	Time(seconds)	Error Distance (m)
Source Location	36.0243282561	-84.1901636495		
Tier 1	36.0240821	-84.1904461	1324.38	37.34
Tier 1B			15.07	
Tier 2	36.0241916	-84.1902256	466.26	16.16
Tier 3	36.0242986	-84.1902022	644.61	4.79

Table D.3: Bayesian Area Exclusion Comparison

Bayesian Threshold Not Met				
Title	Time(seconds)		Error Distance (m)	
Source Location				
Tier 1	2704.58		24.8	
Tier 2	527.47		14.7	
Tier 3	646.30		16.5	
Bayesian Threshold Met				
Title	Time(seconds)	Difference in Time(%)	Error Distance (m)	Difference in Estimate Error(%)
Source Location				
Tier 1	1324.38	-51.03%	37.34	50.56%
Tier 1B	15.07			
Tier 2	466.26	-11.61%	16.16	9.92%
Tier 3	644.61	-0.26%	4.79	-71.00%

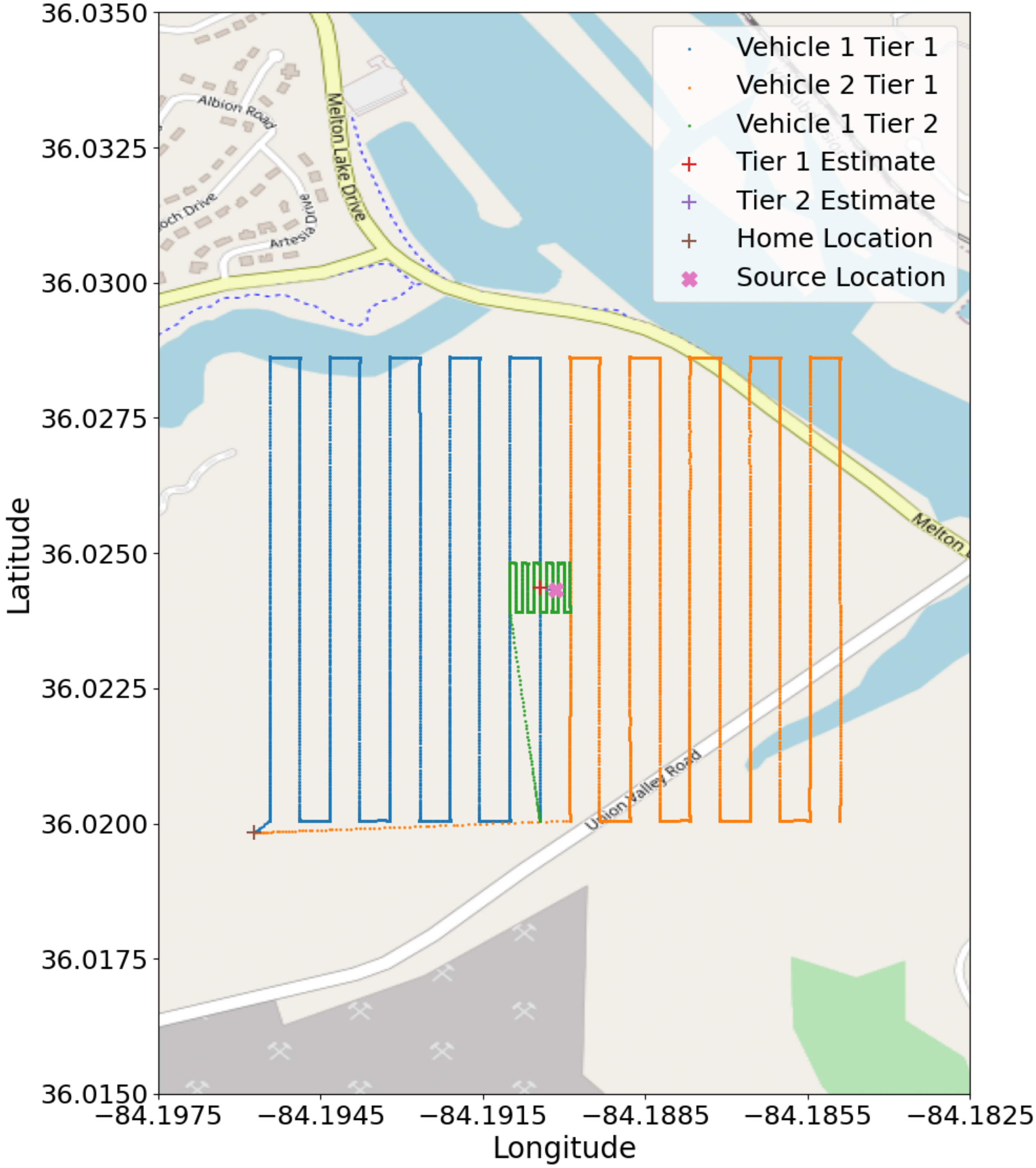

Figure D.5: Flight Path of 2 Drones 50 m alt 10 mCi Centered Source

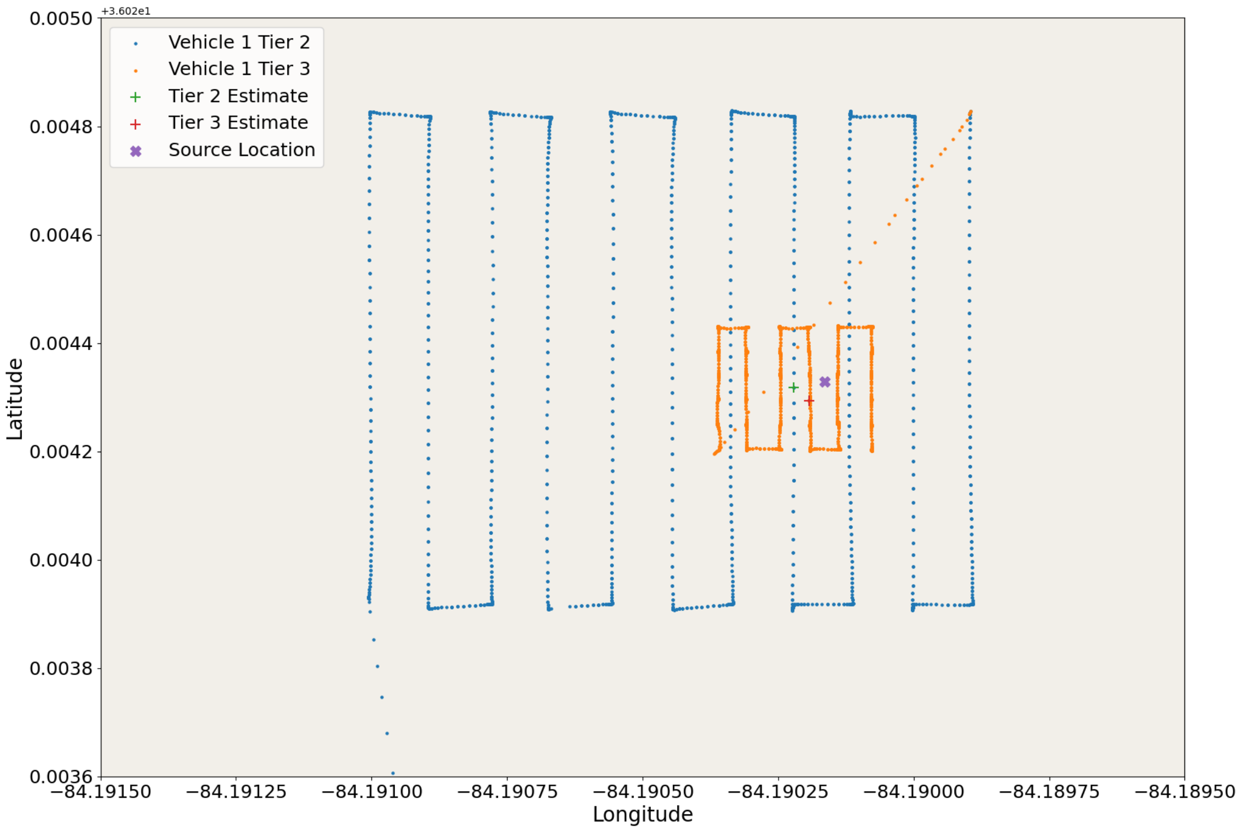

Figure D.6: Flight Path of 2 Drones 50 m alt 10 mCi Centered Source

Table D.4: Two Drones 50m Alt 10 mCi Cs-137 Centered Source

Title	Latitude	Longitude	Time(seconds)	Error Distance (m)
Source Location	36.0243282561	-84.1901636495		
Tier 1	36.0243683	-84.190448	1434.24	26.03
Tier 2	36.0243175	-84.1902207	512.64	5.28
Tier 3	36.0242932	-84.1901924	660.87	4.67

Table D.5: Single vs Multiple Drones Comparison

Single Drone				
Title	Time(seconds)		Error Distance (m)	
Source Location				
Tier 1	2704.58		24.8	
Tier 2	527.47		14.7	
Tier 3	646.30		16.5	
2 Drones				
Title	Time(seconds)	Difference in Time(%)	Error Distance (m)	Difference in Estimate Error(%)
Source Location				
Tier 1	1434.24	-46.97%	26.03	4.96%
Tier 2	512.64	-2.81%	5.28	-64.09%
Tier 3	660.87	2.26%	4.67	-71.67%

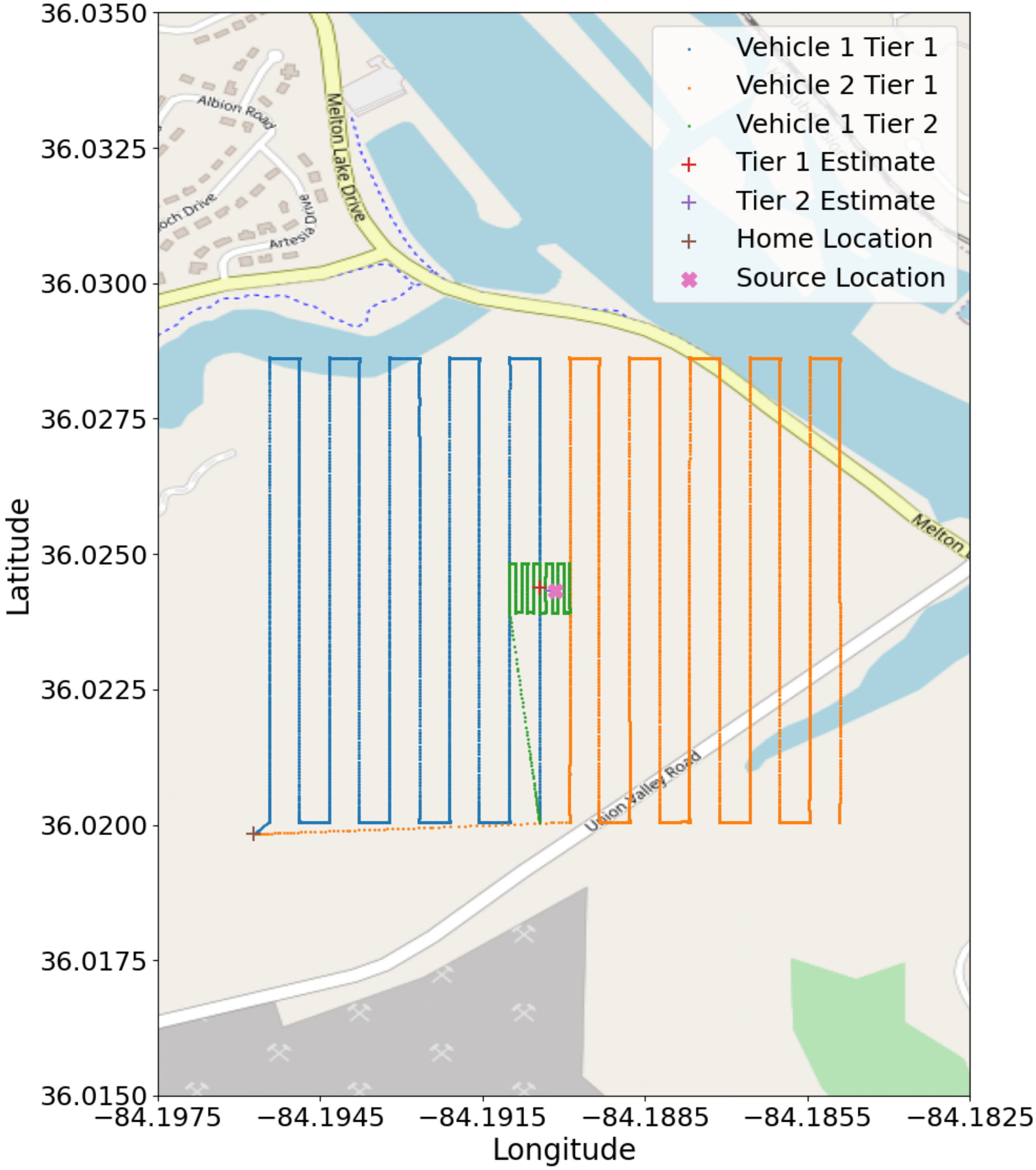

Figure D.7: Flight Path of 2 Drones 25 m alt 10 mCi Centered Source

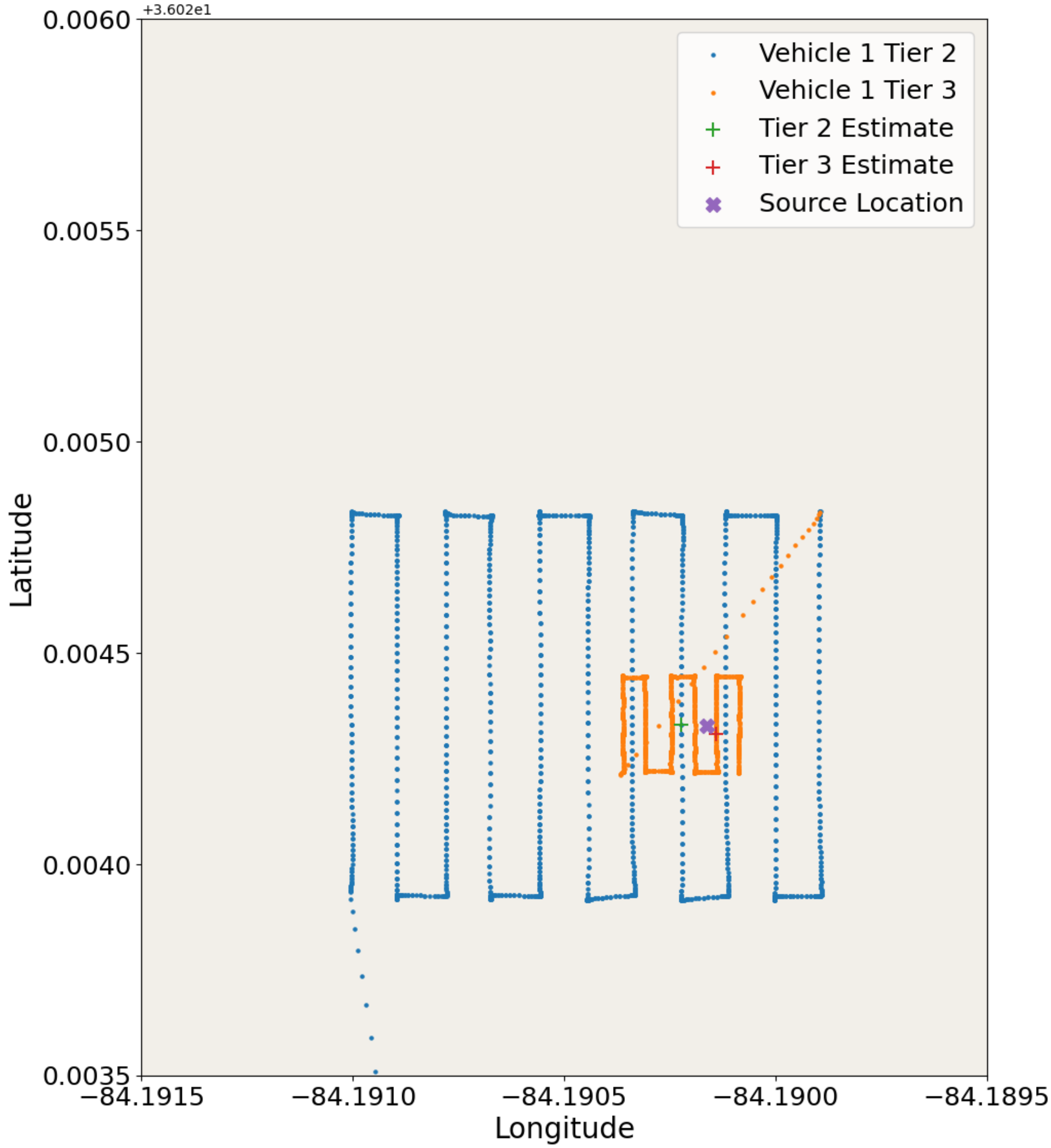

Figure D.8: Flight Path of 2 Drones 25 m alt 10 mCi Centered Source

Table D.6: Two Drones 25 m Altitude Centered 10 mCi Cs-137 source

Title	Latitude	Longitude	Time(seconds)	Error Distance (m)
Source Location	36.0243282561	-84.1901636495		
Tier 1	36.0243751	-84.1904483	1431.29	26.18
Tier 2	36.0243315	-84.1902224	536.31	5.31
Tier 3	36.0243088	-84.1901404	658.06	3.09

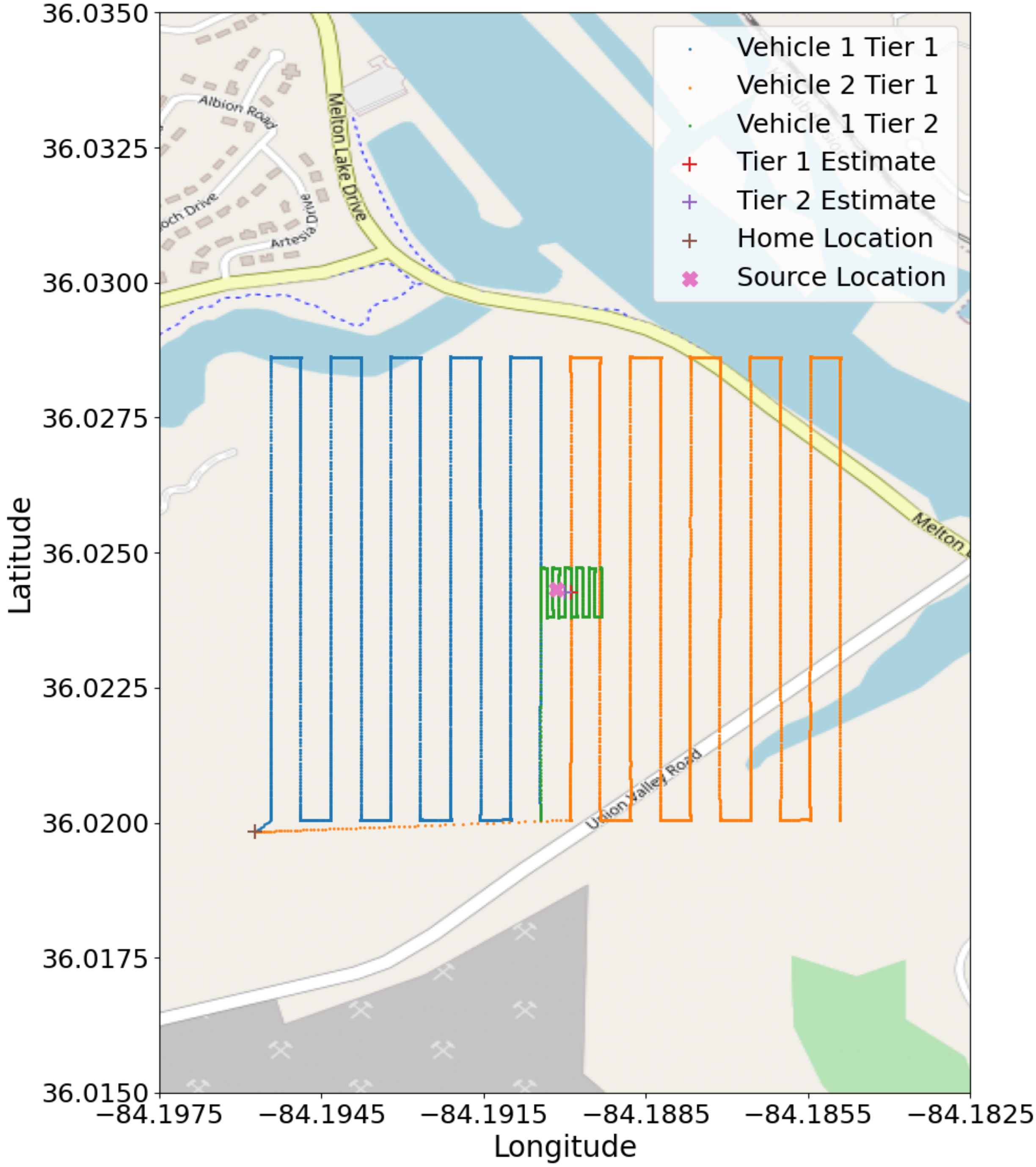

Figure D.9: Flight Path of 2 Drones 75 m alt 10 mCi Centered Source

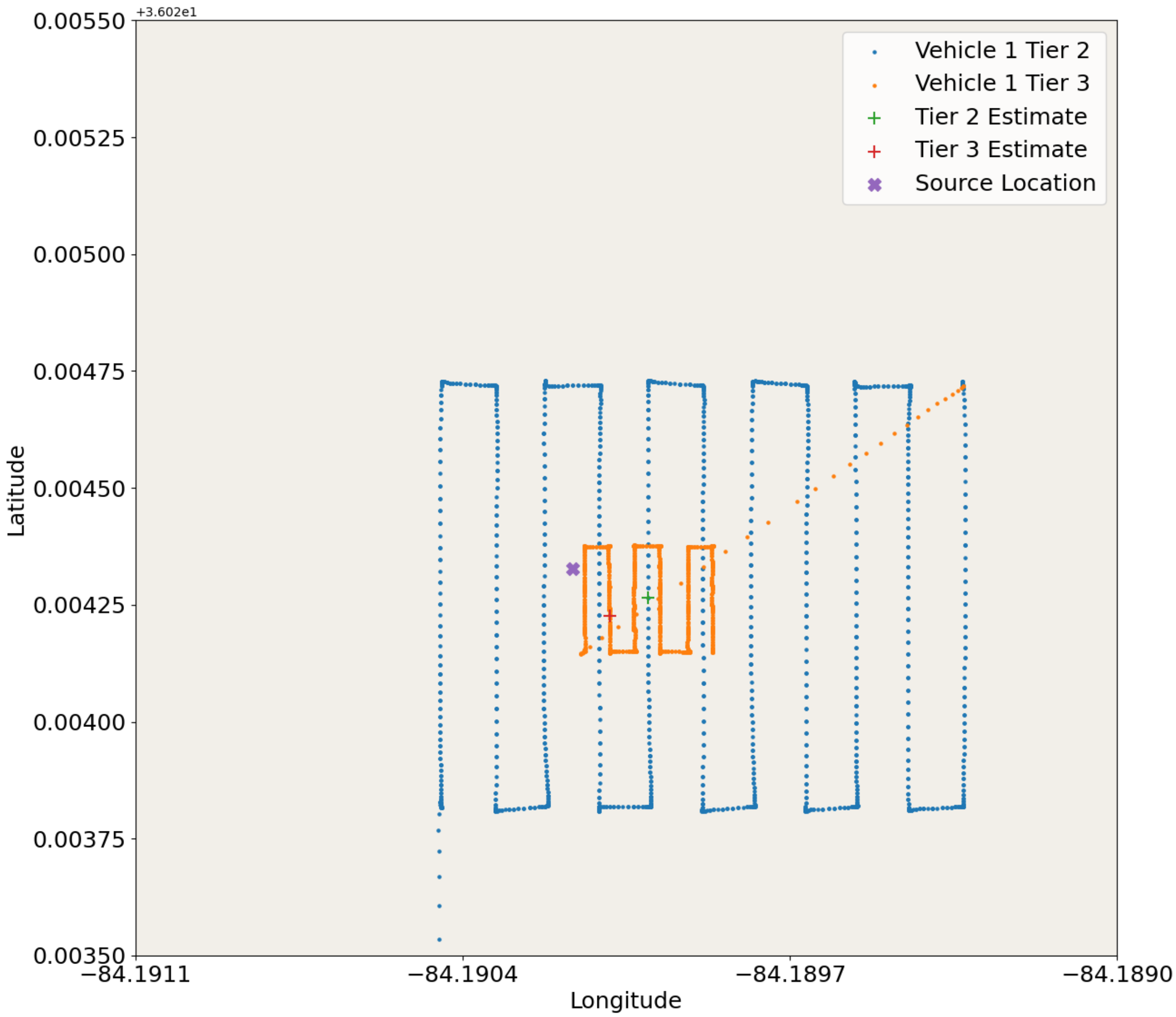

Figure D.10: Flight Path of 2 Drones 75 m alt 10 mCi Centered Source

Table D.7: Two Drone 75 m Altitude Centered 10 mCi Cs-137 source

Title	Latitude	Longitude	Time(seconds)	Error Distance (m)
Source Location	36.0243282561	-84.1901636495		
Tier 1	36.0242689	-84.1898891	1465.4	25.61
Tier 2	36.0242647	-84.190004	524.04	16.03
Tier 3	36.0242261	-84.1900856	666.67	13.34

Table D.8: Altitude Comparison

50 m				
Title	Time(seconds)		Error Distance (m)	
Tier 1	1434.24		26.03	
Tier 2	512.64		5.28	
Tier 3	660.87		4.67	
25 m				
Title	Time(seconds)	Difference in Time(%)	Error Distance (m)	Difference in Estimate Error(%)
Tier 1	1431.29	-0.21%	26.18	0.57%
Tier 2	536.31	4.62%	5.31	0.54%
Tier 3	658.06	-0.43%	3.01	-35.63%
75 m				
Title	Time(seconds)	Difference in Time(%)	Error Distance (m)	Difference in Estimate Error(%)
Tier 1	1465.49	2.18%	25.61	-1.62%
Tier 2	524.04	2.22%	16.03	203.57%
Tier 3	666.67	0.88%	13.34	185.43%

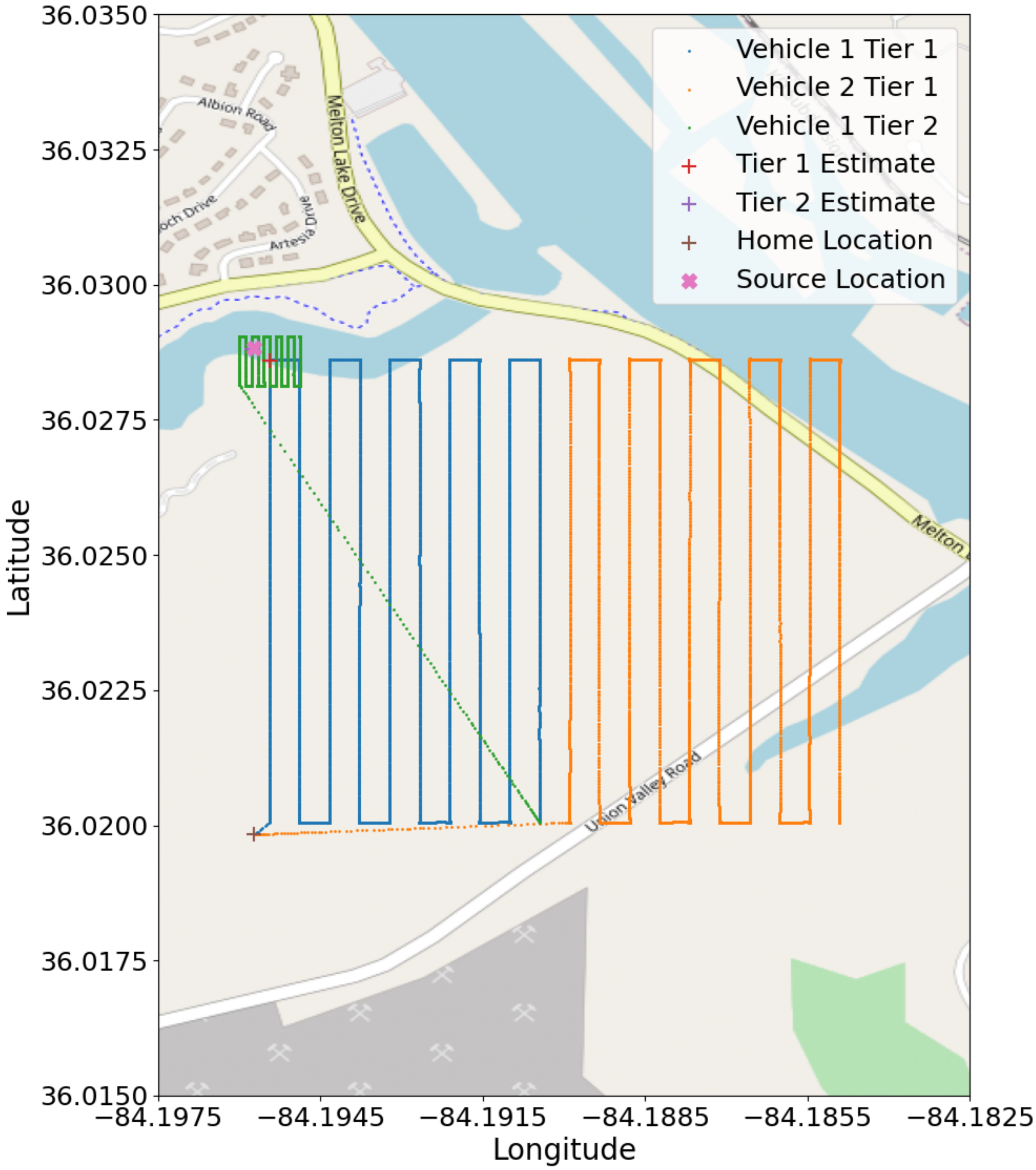

Figure D.11: Flight Path of 2 Drones 50 m alt 10 mCi North East Corner Source

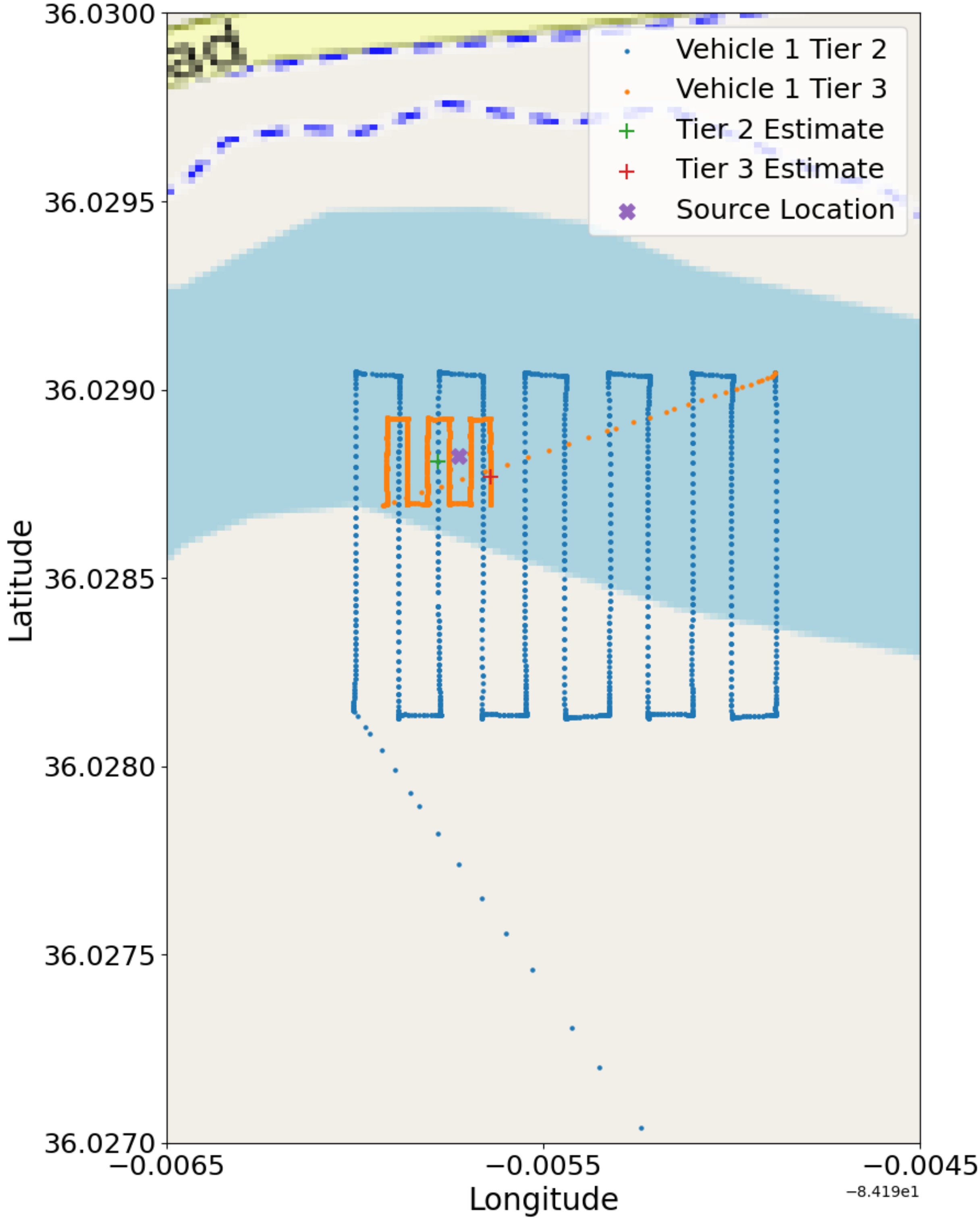

Figure D.12: Flight Path of 2 Drones 50 m alt 10 mCi North East Corner Source

Table D.9: North East Corner Source

Title	Latitude	Longitude	Time(seconds)	Error Distance (m)
Source Location	36.0288249924	-84.1957231611		
Tier 1	36.0285887	-84.1954416	1472.42	36.49
Tier 2	36.0288103	-84.1957787	560.88	5.26
Tier 3	36.028768	-84.1956402	667.56	9.79

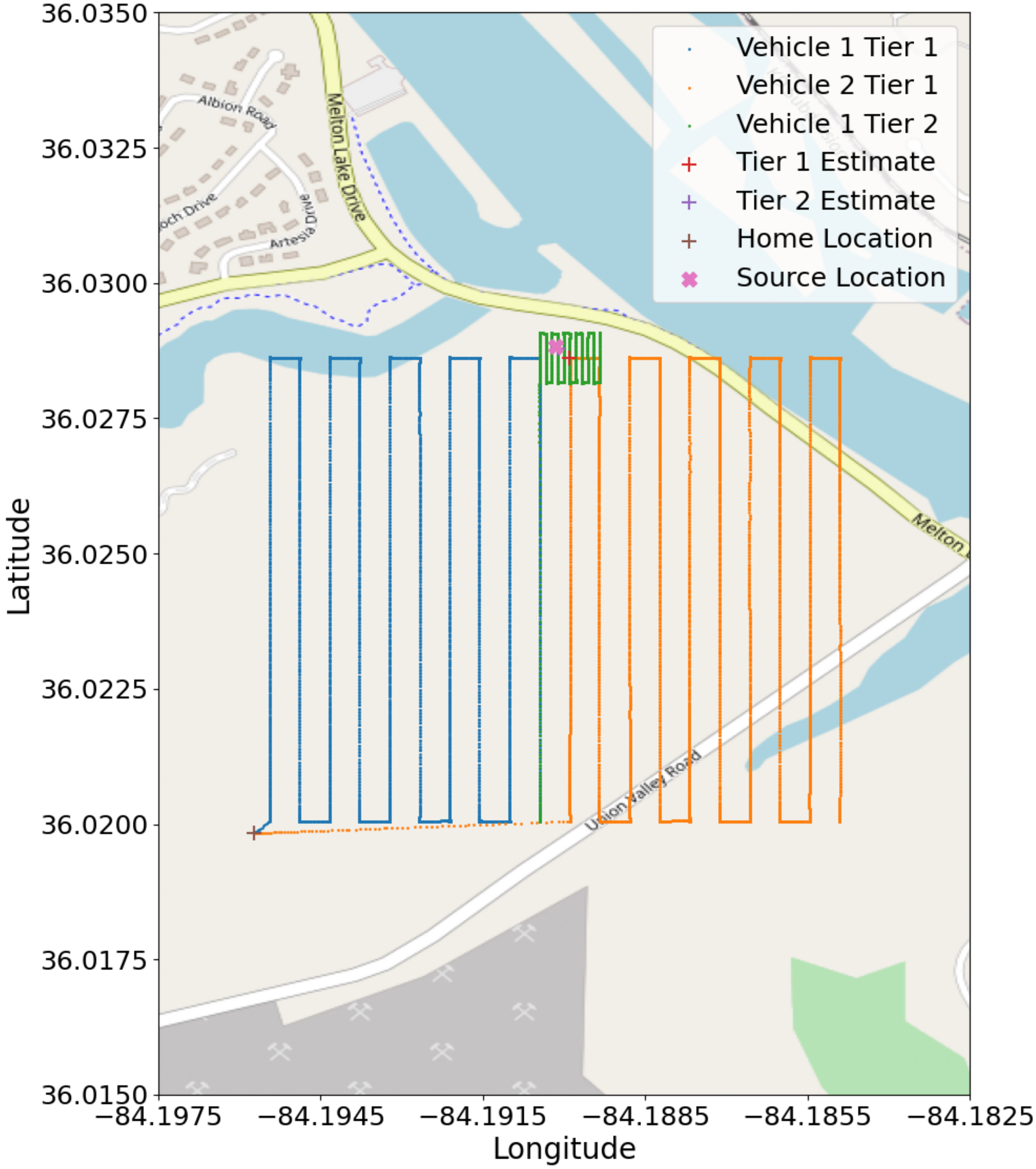

Figure D.13: Flight Path of 2 Drones 50 m alt 10 mCi Centered Northern Edge Source

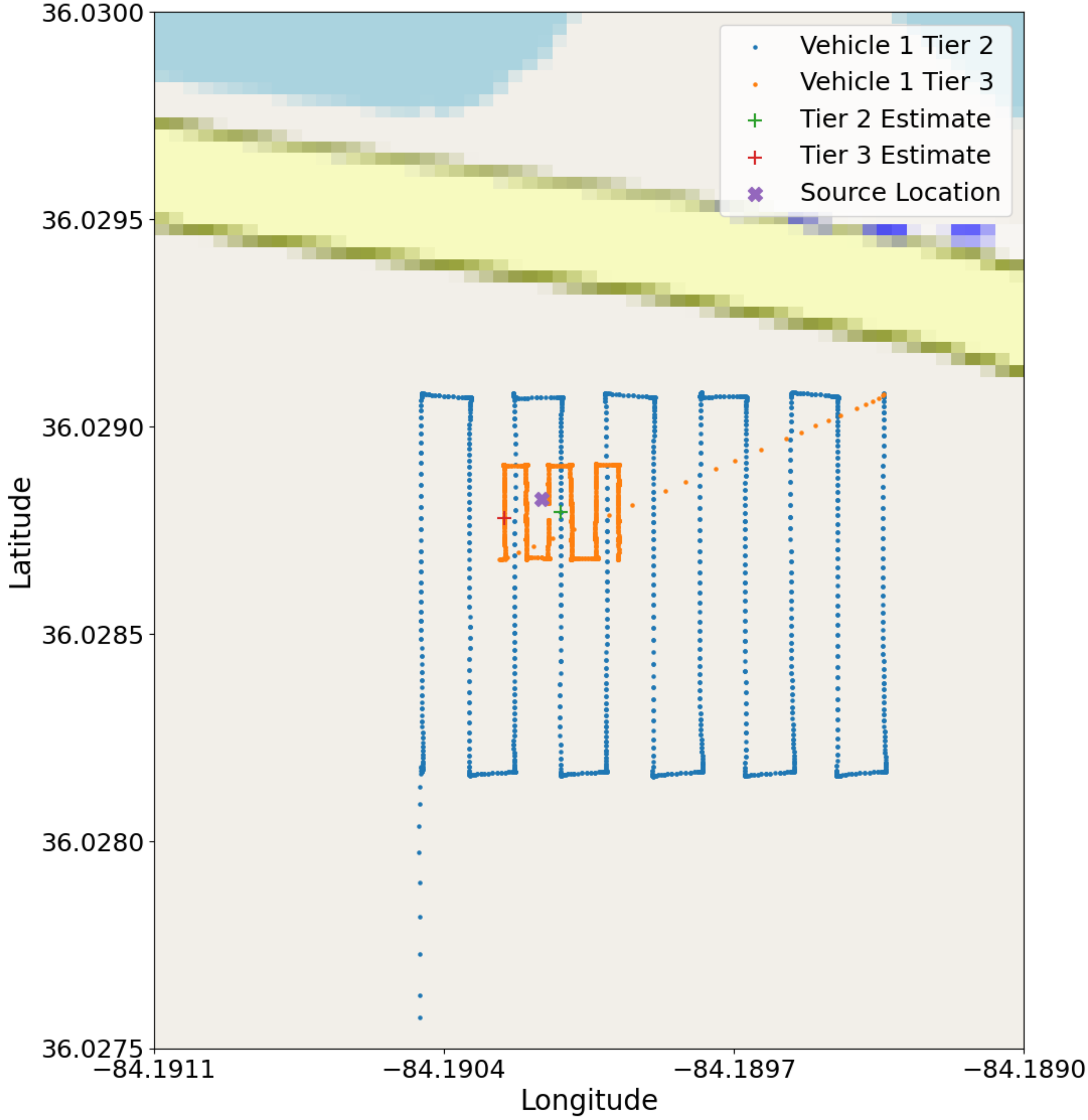

Figure D.14: Flight Path of 2 Drones 50 m alt 10 mCi Centered Northern Edge Source

Table D.10: Centered Northern Edge Source

Title	Latitude	Longitude	Time(seconds)	Error Distance (m)
Source Location	36.0288248641	-84.1901636495		
Tier 1	36.0286196	-84.1898954	1432.12	33.26
Tier 2	36.028795	-84.1901184	545.25	5.25
Tier 3	36.0287792	-84.1902535	652.74	9.55

Table D.11: Source Position Comparison

Centered				
Title	Time(seconds)		Error Distance (m)	
Tier 1	1434.24		26.03	
Tier 2	512.64		5.28	
Tier 3	660.87		4.67	
North West				
Title	Time(seconds)	Difference in Time(%)	Error Distance (m)	Difference in Estimate Error(%)
Tier 1	1472.42	2.66%	36.49	40.18%
Tier 2	560.88	9.41%	5.26	-0.27%
Tier 3	667.56	1.01%	9.79	109.52%
Centered North Edge				
Title	Time(seconds)	Difference in Time(%)	Error Distance (m)	Difference in Estimate Error(%)
Tier 1	1432.12	-0.15%	33.22	27.61%
Tier 2	545.25	6.36%	5.25	-0.46%
Tier 3	652.74	-1.23%	9.55	104.38%

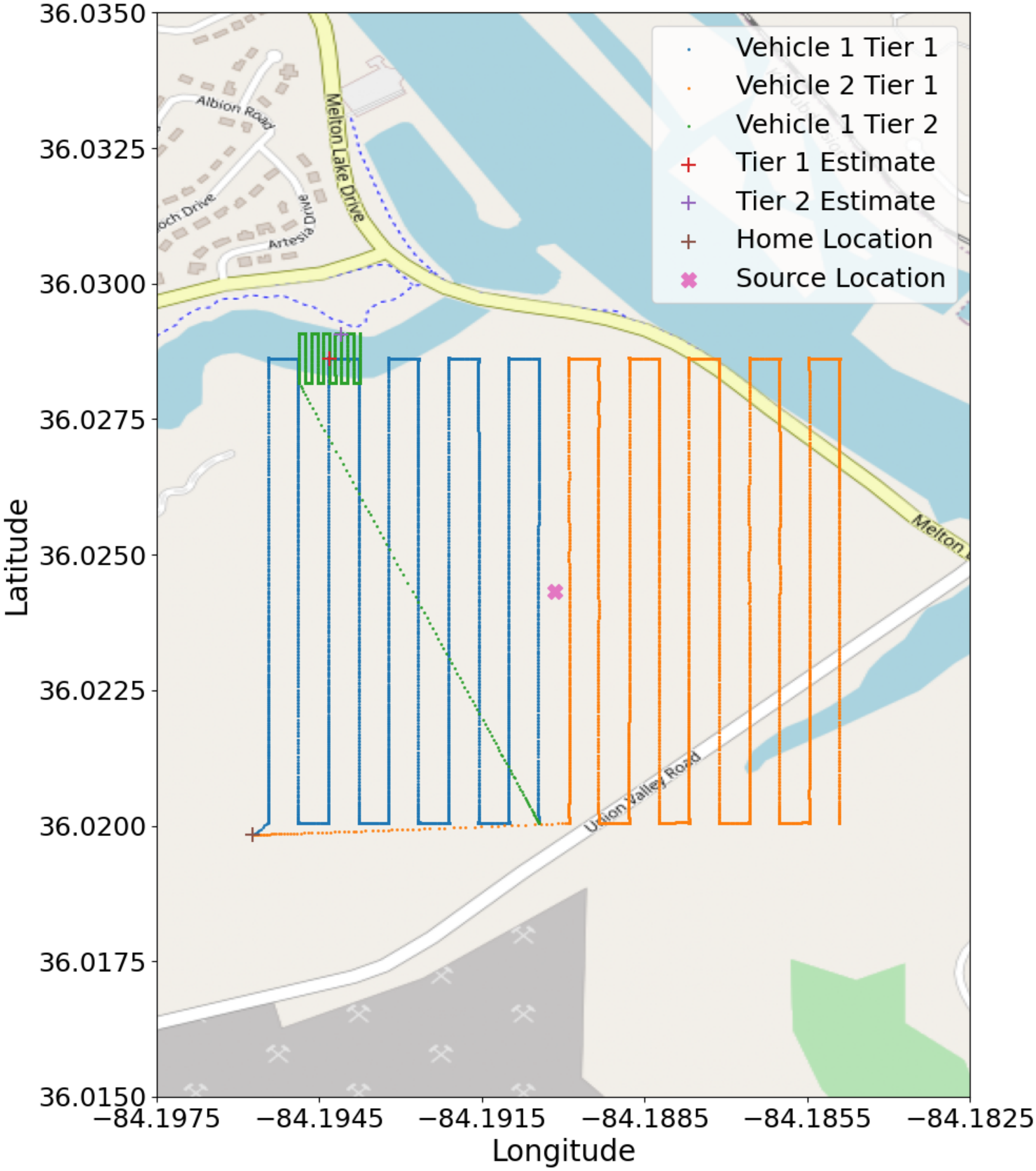

Figure D.15: Flight Path of 2 Drones 50 m alt 0.1 mCi Centered Source

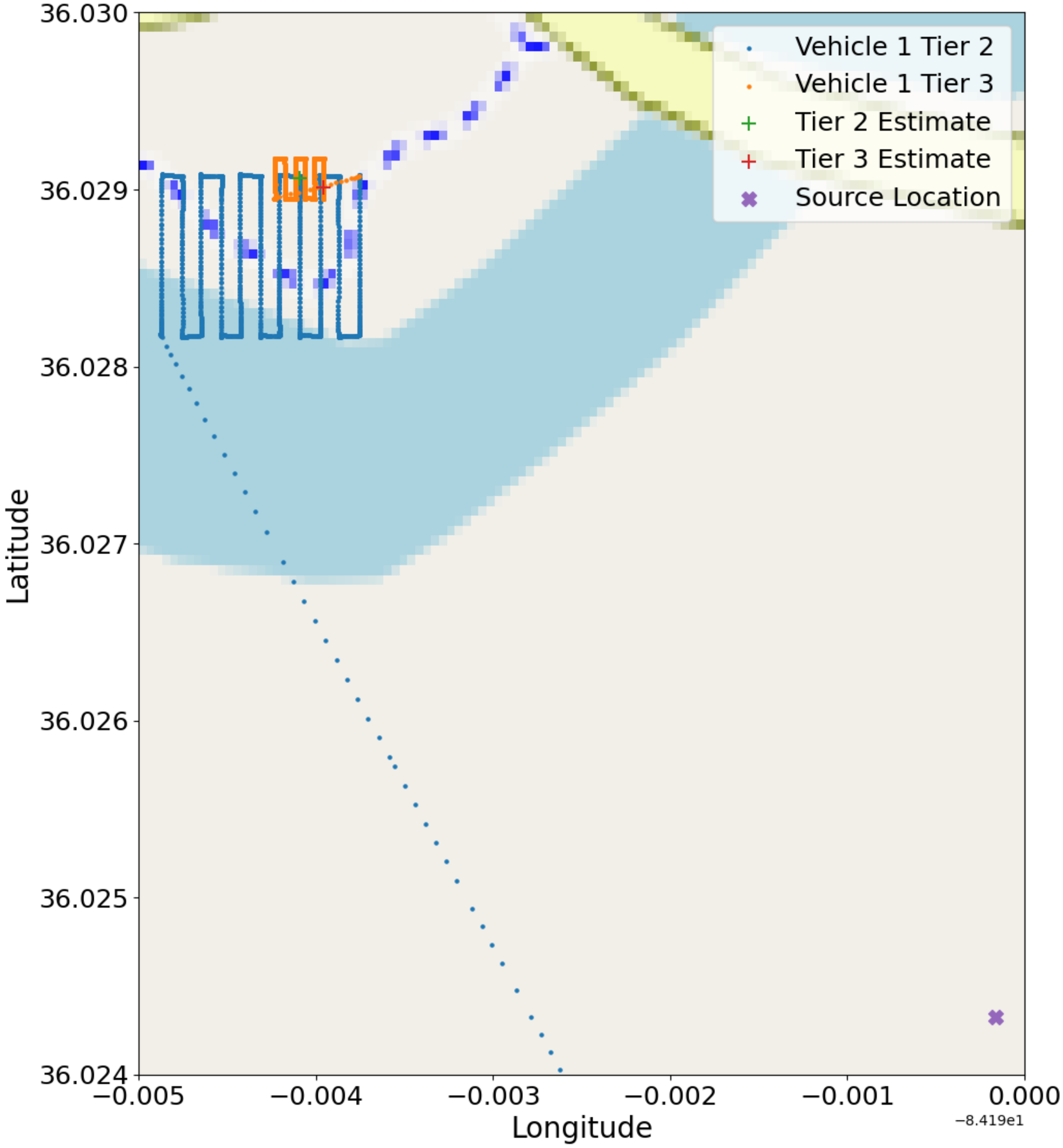

Figure D.16: Flight Path of 2 Drones 50 m alt 0.1 mCi Centered Source

Table D.12: 50 m 0.1 mCi

Title	Latitude	Longitude	Time(seconds)	Error Distance (m)
Source Location	36.0243282561	-84.1901636495		
Tier 1	36.0286258	-84.1943134	1452.49	606.04
Tier 2	36.0290633	-84.1940901	577.79	633.48
Tier 3	36.0290132	-84.1939553	648.63	622.12

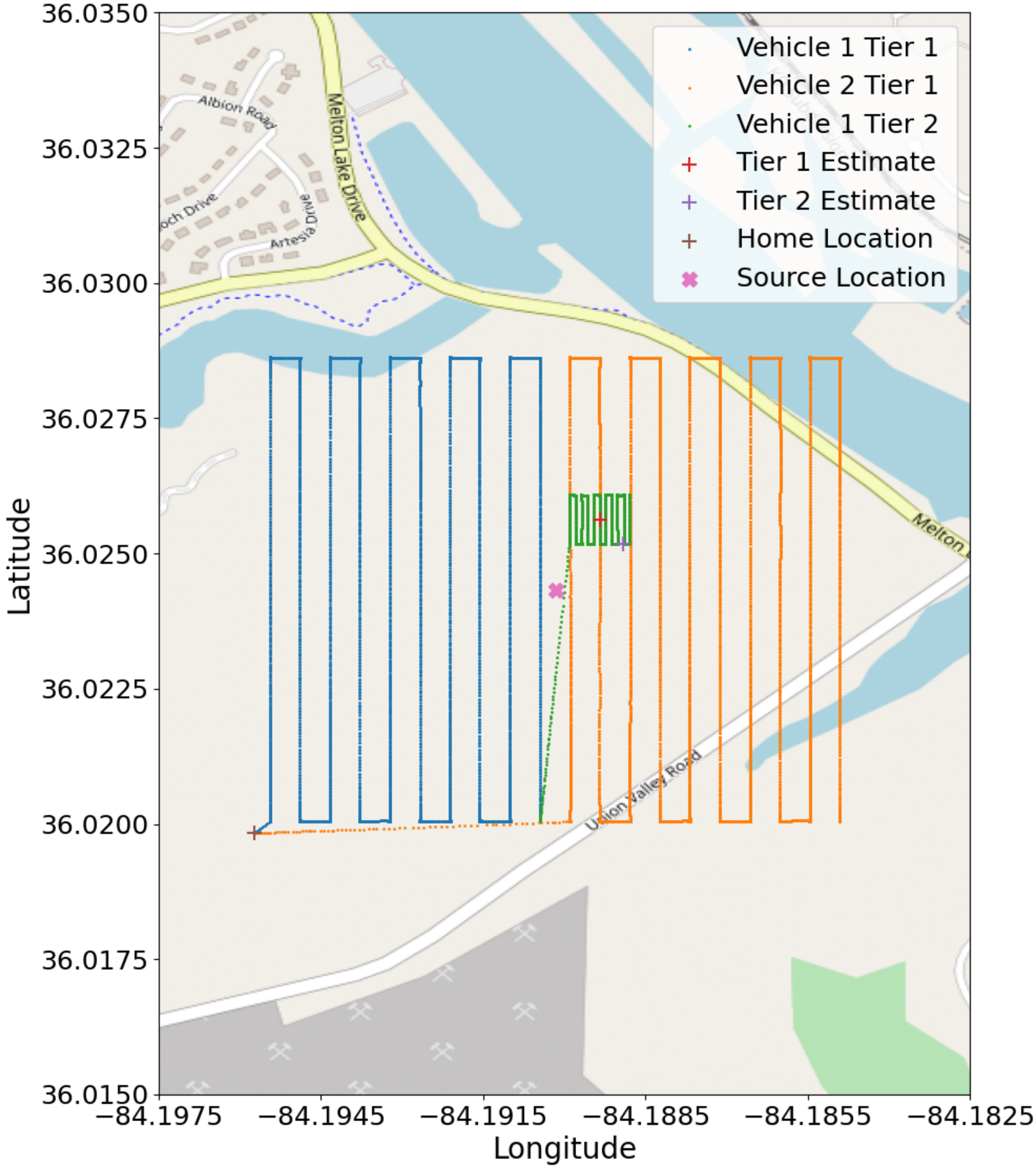

Figure D.17: Flight Path of 2 Drones 25 m alt 0.1 mCi Centered Source

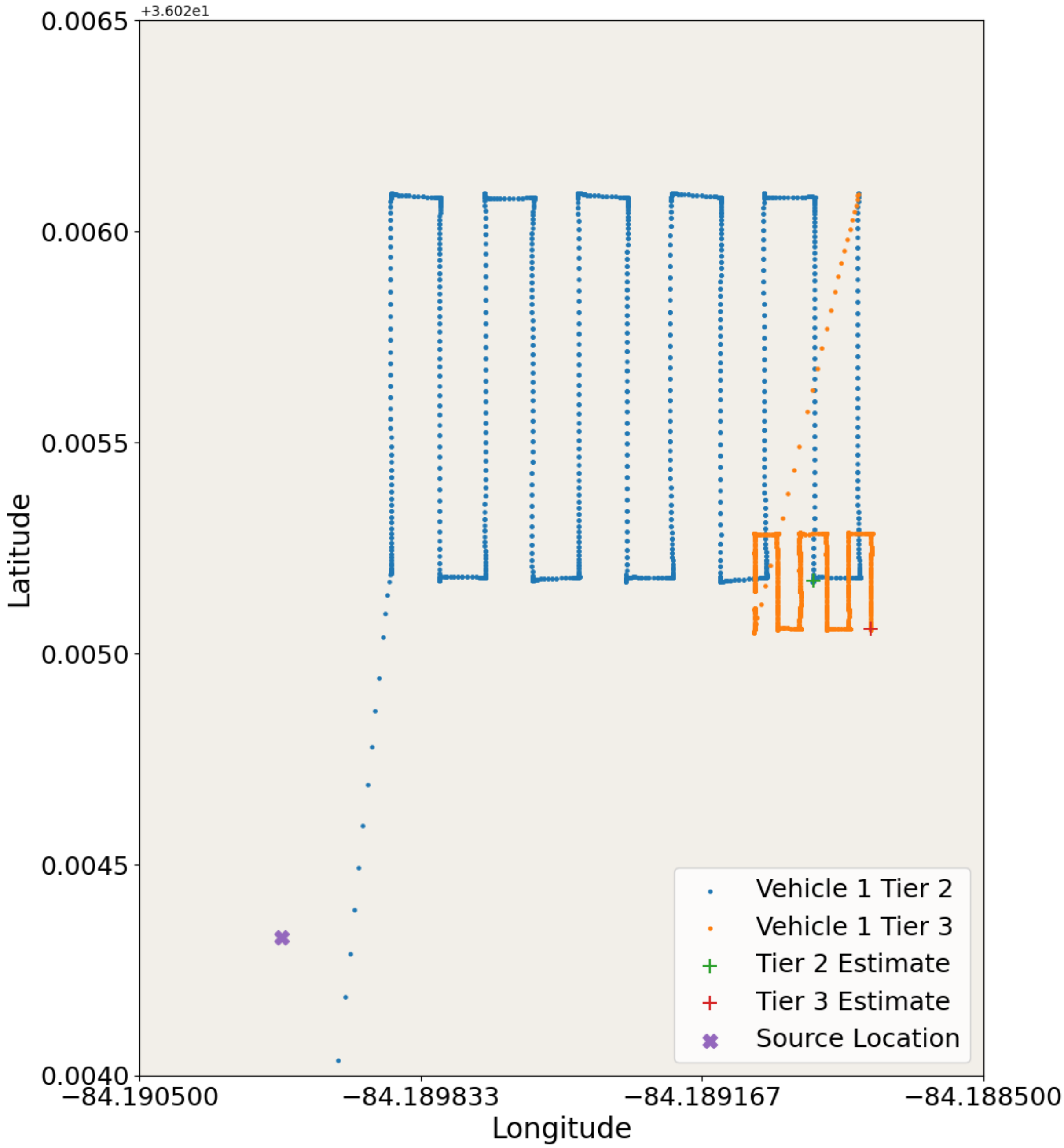

Figure D.18: Flight Path of 2 Drones 25 m alt 0.1 mCi Centered Source

Table D.13: 25 m 0.1 mCi

Title	Latitude	Longitude	Time(seconds)	Error Distance (m)
Source Location	36.0243282561	-84.1901636495		
Tier 1	36.0256301	-84.1893488	1448.05	162.05
Tier 2	36.025172	-84.1889034	534.61	147.20
Tier 3	36.0250592	-84.1887675	659.17	149.71

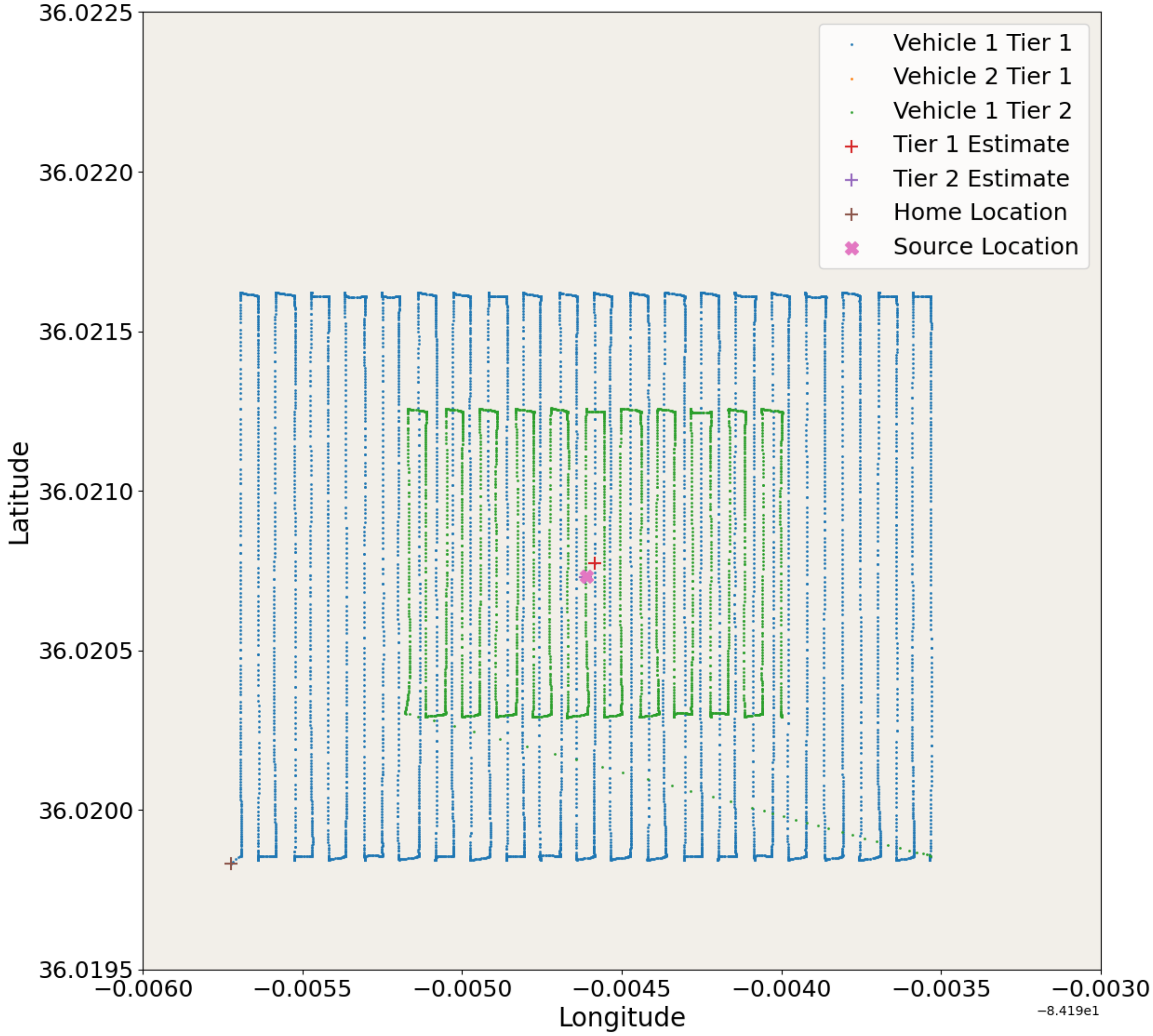

Figure D.19: Flight Path of 2 Drones 6.75 m alt 0.1 mCi Centered Source

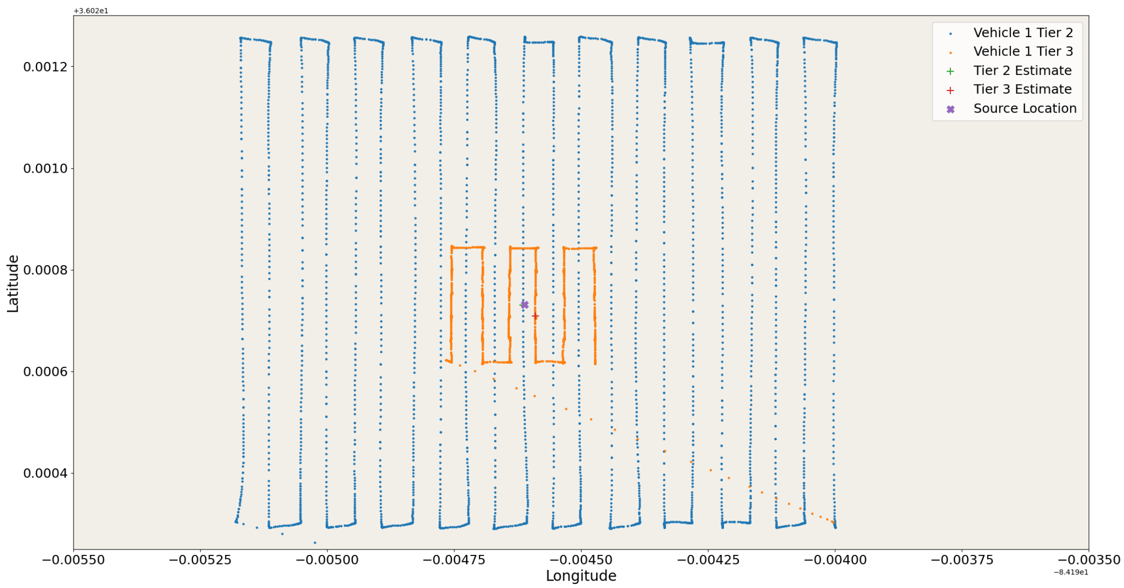

Figure D.20: Flight Path of 2 Drones 6.75 m alt 0.1 mCi Centered Source

Table D.14: 6.75 m 0.1 mCi

Title	Latitude	Longitude	Time(seconds)	Error Distance (m)
Source Location	36.0207311	-84.1946113		
Tier 1	36.0207745	-84.1945847	2067.73	5.38
Tier 2	36.0207302	-84.1946142	878.39	0.28
Tier 3	36.0207085	-84.1945899	648.50	3.16

Table D.15: 0.1 mCi Source Comparison

50 m 10 mCi				
Title	Time(sec)		Error Distance (m)	
Tier 1	1434.24		26.03	
Tier 2	512.64		5.28	
Tier 3	660.87		4.67	
50 m				
Title	Time(sec)	Time Diff. (%)	Error Distance (m)	Est. Error Diff. (%)
Tier 1	1452.48	1.27%	606.04	2228.23%
Tier 2	577.79	12.71%	633.48	11899.94%
Tier 3	648.63	-1.85%	622.12	13210.16%
25 m				
Title	Time(sec)	Time Diff. (%)	Error Distance (m)	Est. Error Diff. (%)
Tier 1	1448.05	0.96%	162.05	522.55%
Tier 2	534.61	4.29%	147.20	2688.45%
Tier 3	659.17	-0.26%	149.71	3103.14%
6.75 m				
Title	Time(sec)	Time Diff. (%)	Error Distance (m)	Est. Error Diff. (%)
Tier 1	2067.73	44.17%	5.38	-79.34%
Tier 2	878.39	71.35%	0.28	-94.64%
Tier 3	648.50	-1.87%	3.16	-32.37%

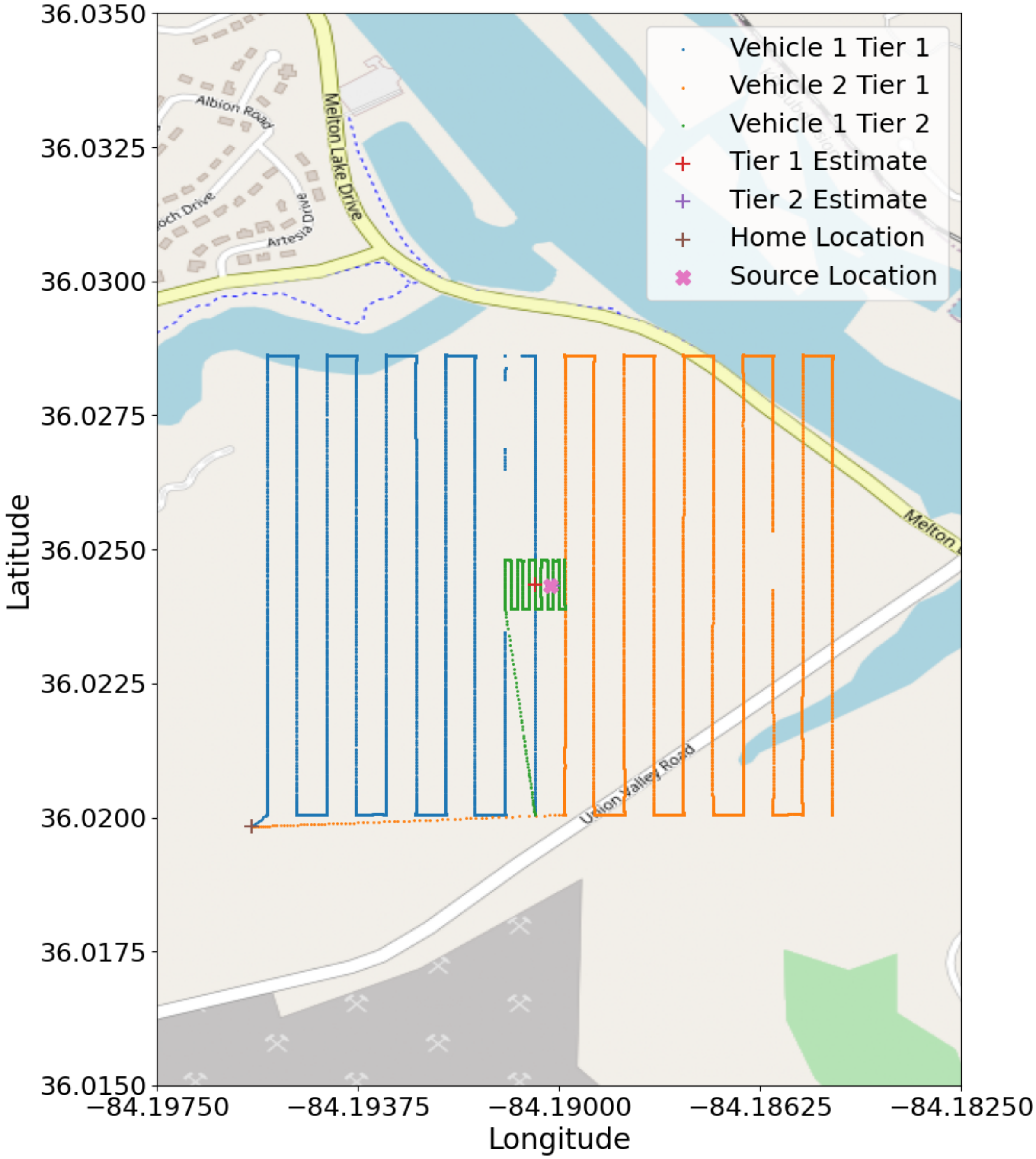

Figure D.21: Flight Path of 2 Drones 50 m alt 1000 mCi Centered Source

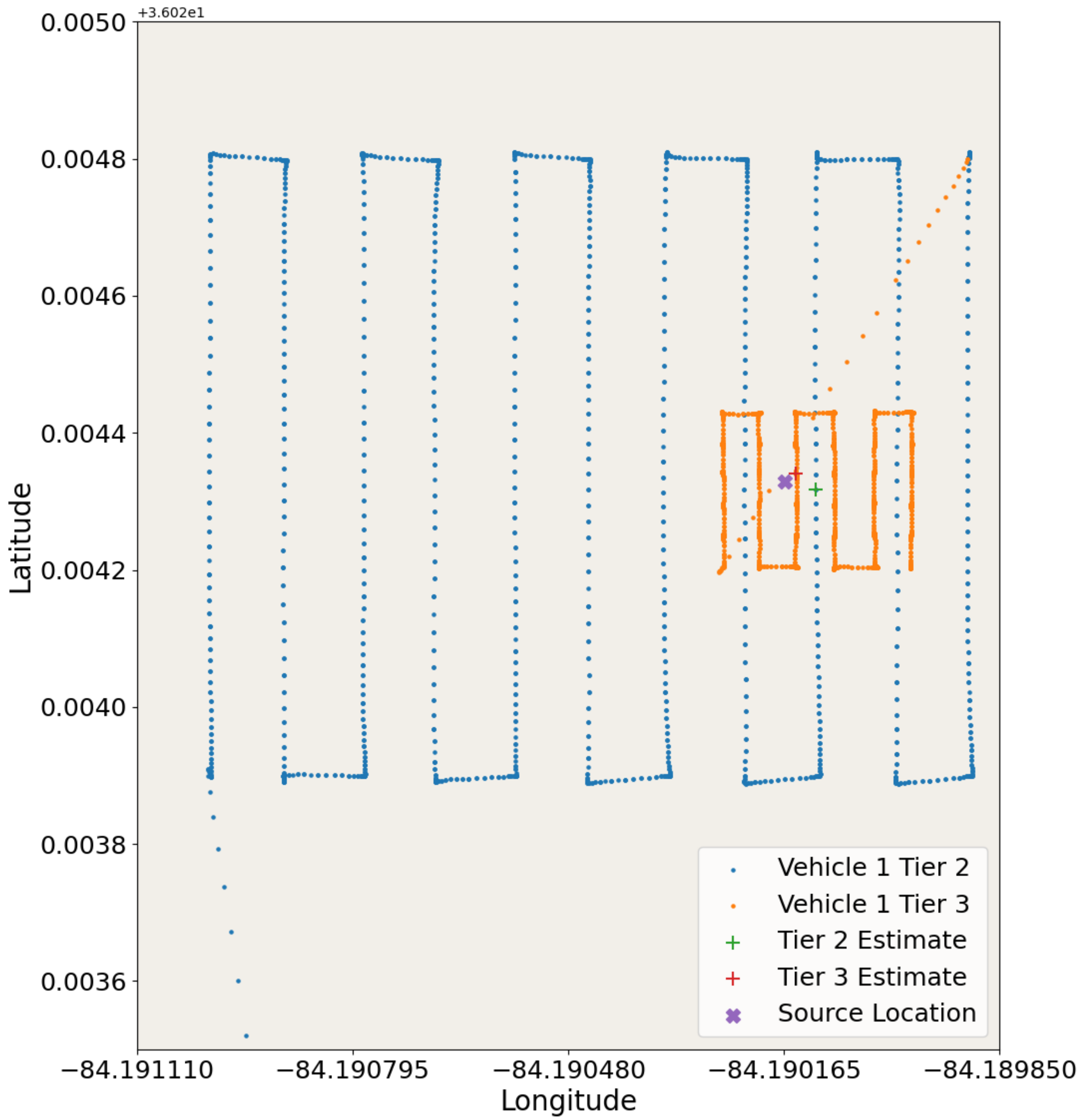

Figure D.22: Flight Path of 2 Drones 50 m alt 1000 mCi Centered Source

Table D.16: 50 m 1000 mCi

Title	Latitude	Longitude	Time(seconds)	Error Distance (m)
Source Location	36.0243282561	-84.19		
Tier 1	36.0286258	-84.19	1452.49	606.04
Tier 2	36.0290633	-84.19	577.79	633.47
Tier 3	36.0290132	-84.19	648.63	622.12

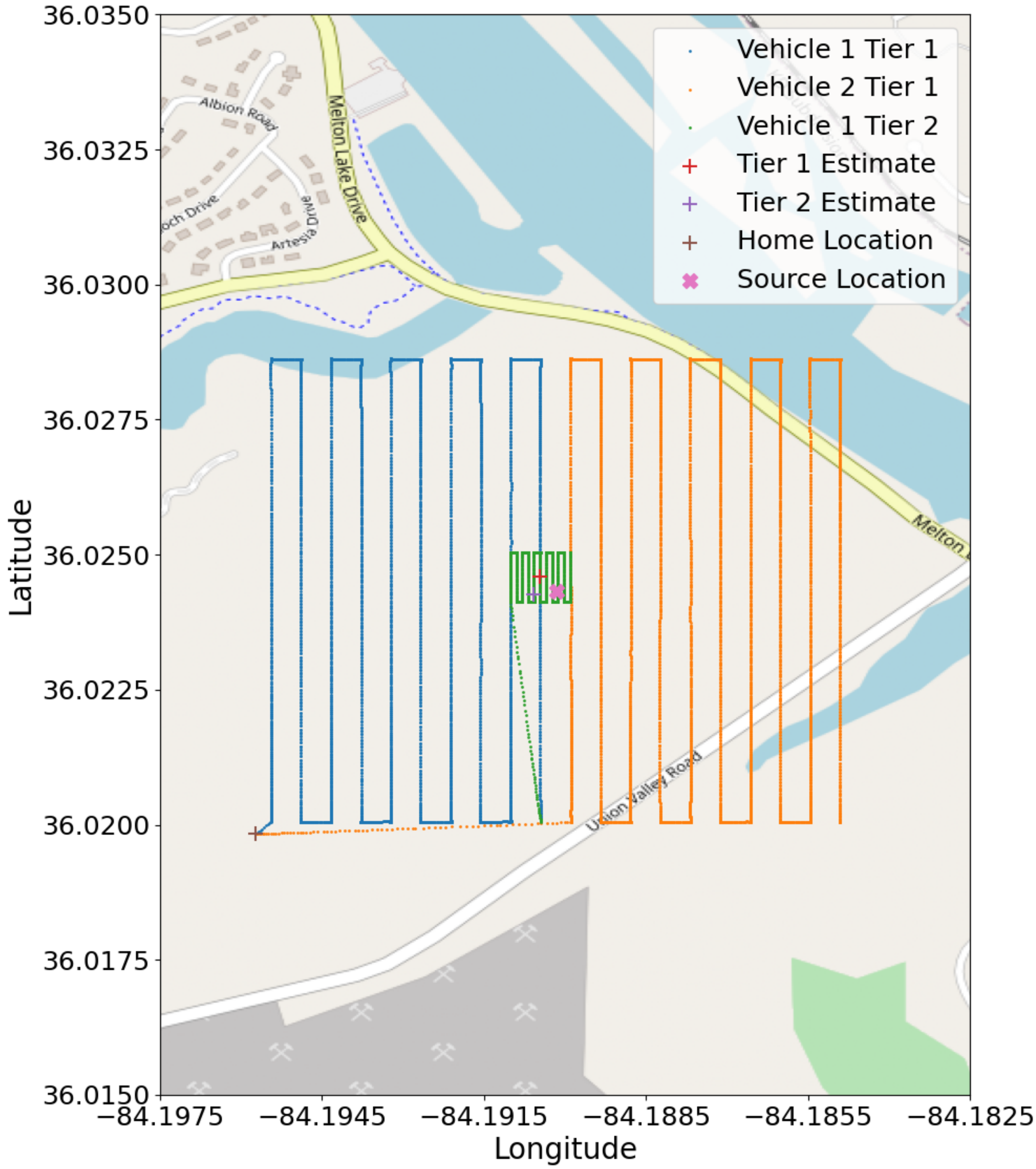

Figure D.23: Flight Path of 2 Drones 248 m alt 1000 mCi Centered Source

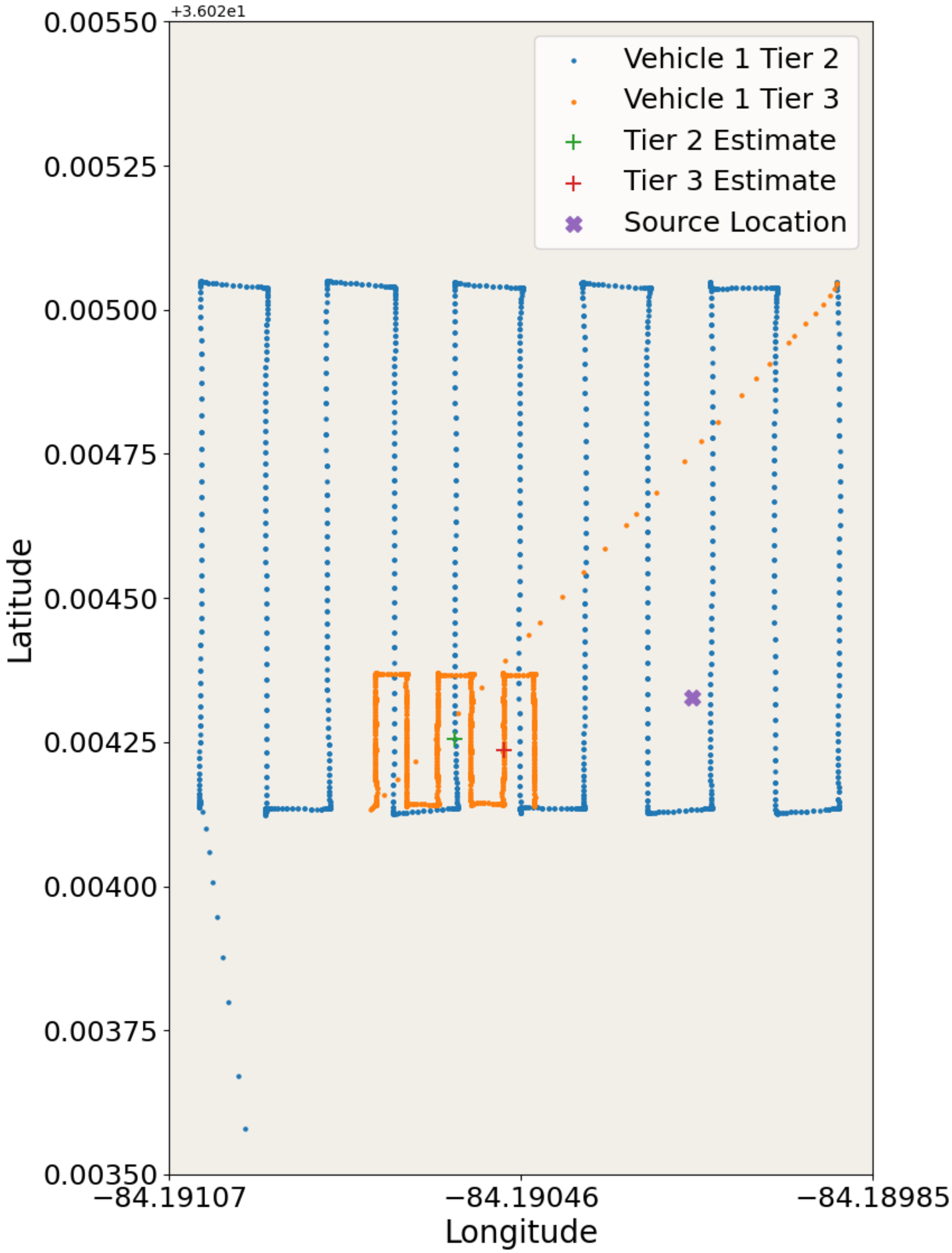

Figure D.24: Flight Path of 2 Drones 248 m alt 1000 mCi Centered Source

Table D.17: 248 m 1000 mCi

Title	Latitude	Longitude	Time(seconds)	Error Distance (m)
Source Location	36.0243282561	-84.1901636495		
Tier 1	36.0245876	-84.190462	1562.01	39.39
Tier 2	36.0242565	-84.1905739	513.68	37.83
Tier 3	36.0242352	-84.1904897	672.09	31.15

Table D.18: 1000 mCi Source Comparison

50 m 10 mCi				
Title	Time(seconds)		Error Distance (m)	
Tier 1	1434.24		26.03	
Tier 2	512.64		5.28	
Tier 3	660.87		4.67	
50 m 1000 mCi				
Title	Time(seconds)	Difference in Time(%)	Error Distance (m)	Difference in Estimate Error(%)
Tier 1	1471.75	2.62%	25.82	-0.79%
Tier 2	520.17	1.47%	4.22	-20.00%
Tier 3	651.82	-1.37%	1.99	-57.52%
248 m 1000 mCi				
Title	Time(seconds)	Difference in Time(%)	Error Distance (m)	Difference in Estimate Error(%)
Tier 1	1562.01	8.91%	39.39	51.31%
Tier 2	513.67873	0.20%	37.83	616.54%
Tier 3	672.09	1.70%	31.15	566.45%

Vita

William Lynch is from Nashville, TN. In 2015, he graduated Montgomery Bell Academy and proceeded to attend the University of Tennessee, Knoxville for his Bachelor of Science degree in nuclear engineering. He worked at Oak Ridge National Lab Radiochemical Engineering Development Center as a member of a Californium-252 recovery operation. His current work includes research for the Institute for Nuclear Security at the University of Tennessee while completing his Master of Science degree in nuclear engineering. Aspirations include working in nuclear control and monitoring systems.